








Inhibition of urothelial carcinoma through targeted type I interferon-mediated immune activation

Devin Plote ^{a,b}, Woonyoung Choi^c, Sharada Mokkapati ^d, Debasish Sundi ^e, James E Ferguson III ^d, Jon Duplisea^d, Nigel R. Parker^f, Seppo Yla-Herttuala^g, SUO CTC Bladder Committee ^h, David McConkey^c, Kimberly S. Schluns ^b, and Colin P. Dinney ^d

^aCancer Biology Graduate Program, The University of Texas MD Anderson Cancer Center; University of Texas Health Graduate School of Biomedical Sciences at Houston, Houston, TX, USA; ^bDepartment of Immunology, The University of Texas MD Anderson Cancer Center, Houston, TX, USA; ^cJames Buchanan Brady Urological Institute, Johns Hopkins Greenberg Bladder Cancer Institute, Johns Hopkins University, School of Medicine, Baltimore, MD, USA; ^dDepartment of Urology, The University of Texas MD Anderson Cancer Center, Houston, TX, USA; ^eDepartment of Urology, The Ohio State University Comprehensive Cancer Center, Columbus, OH, USA; ^fMiddlesex, Hamesman, Ltd., Edgware, London, UK; ^gA.I. Virtanen Institute for Molecular Sciences, University of Eastern Finland, Kuopio, Finland; ^hSociety of Urologic Oncology Clinical Trials Consortium, Schaumburg, IL, USA

ABSTRACT

Type I interferon (IFN-I) has potent anti-tumor effects against urothelial carcinoma (UC) and may be an alternative treatment option for patients who do not respond to Bacillus Calmette-Guerin. However, the mechanisms that mediate the IFN-I-stimulated immune responses against UC have yet to be elucidated. Herein, we evaluated the anti-tumor mechanisms of IFN-I in UC in human patients and in mice. Patient tumors from a Phase I clinical trial with adenoviral interferon- α (Ad-IFN α /Syn3) showed increased expression of T cell and checkpoint markers following treatment with Ad-IFN α /Syn3 by RNAseq and immunohistochemistry analysis in 25% of patients. In mice, peritumoral injections of poly(I:C) into MB49 UC tumors was used to incite an IFN-driven inflammatory response that significantly inhibited tumor growth. IFN-I engaged both innate and adaptive cells, seen in increased intratumoral CD8 T cells, NK cells, and CD11b⁺Ly6G⁺ cells, but tumor inhibition was not reliant on any one immune cell type. Nonetheless, poly(I:C)-mediated tumor regression and change in the myeloid cell landscape was dependent on IL-6. Mice were also treated with poly(I:C) in combination with anti-PD-1 monoclonal antibody (mAb) to assess for additional benefit to tumor growth and animal survival. When used in combination with anti-PD-1 mAb, IFN-I stimulation prolonged survival, coinciding with inhibition of angiogenesis and enriched gene signatures of metabolism, extracellular matrix organization, and MAPK/AKT signaling. Altogether, these findings suggest IFN-I's immune-driven antitumor response in UC is mediated by IL-6 and a collaboration of immune cells, and its use in combination with checkpoint blockade therapy can increase clinical benefit.

ARTICLE HISTORY

Received 25 July 2018
Revised 4 January 2019
Accepted 24 January 2019

KEYWORDS



PD-1; interferon; bladder cancer; immune microenvironment


Introduction

Non-muscle-invasive bladder cancer (NMIBC) comprises ~70% of diagnosed urothelial carcinomas (UC).¹ Although not immediately life-threatening, they have a propensity to recur and progress. Intravesical therapy, mainly in the form of Bacillus Calmette-Guerin (BCG), is administered to prevent recurrence, delay progression, and provide for bladder preservation to avoid the quality of life issues that accompany radical cystectomy.^{1,2} Despite its success as frontline immunotherapy, not all patients respond to BCG, and of those who do respond, over half will relapse with BCG Unresponsive NMIBC.³⁻⁵ Unfortunately, no effective second-line therapy for BCG Unresponsive NMIBC exists.^{2,4-6} Interferon alpha (IFN α) is a pleiotropic cytokine that inhibits tumor growth directly as well as indirectly through activation of the immune system. These multifaceted anti-tumor properties make IFN α a promising alternative therapy for UC. IFN α monotherapy for NMIBC was previously studied demonstrating good tolerability and dose-related clinical effectiveness

following BCG failure; however, its response durability was insufficient.⁷ With standard intravesical therapy, patients are unable to retain the instilled cytokine for more than 1–2 h, limiting local tumor exposure. To overcome these limitations, intravesical gene delivery of IFN α through the use of adenoviral encoding IFN α (Ad-IFN α /Syn3, i.e. Instiladrin) was developed and early clinical trials have shown its safety and efficacy in treating BCG Unresponsive NMIBC.⁸⁻¹⁰ Clinical studies evaluating the use of intravesical Ad-IFN α /Syn3 in the bladder are ongoing.⁸⁻¹⁰

Because IFN α effects are diverse, its mechanisms of actions have not been fully elucidated in UC. We have previously demonstrated that IFN α gene therapy inhibits the growth of human tumor xenografts by an anti-angiogenic effect and tumor necrosis factor-related apoptosis ligand (TRAIL)-mediated cytotoxicity.¹¹⁻¹⁵ However since these previous preclinical data were generated in studies of nude mice, the immune mechanisms underlying the anti-tumor activity of IFN α in UC

CONTACT Kimberly S. Schluns  kschluns@mdanderson.org  Department of Immunology, The University of Texas MD Anderson Cancer Center, 1515 Holcombe Blvd, Houston, TX 77030, USA

 Supplemental data for this article can be accessed on the [publisher's website](#)

© 2019 The Author(s). Published with license by Taylor & Francis Group, LLC.

This is an Open Access article distributed under the terms of the Creative Commons Attribution-NonCommercial-NoDerivatives License (<http://creativecommons.org/licenses/by-nc-nd/4.0/>), which permits non-commercial re-use, distribution, and reproduction in any medium, provided the original work is properly cited, and is not altered, transformed, or built upon in any way.

have not been defined. Type I interferons (IFN-I), IFN α and interferon-beta (IFN β), promote antigen processing, presentation, and recognition by professional antigen-presenting cells, and induce production of cytokines and chemokines, which in turn recruit and activate a cytotoxic T cell response against the tumor.^{16,17} Preclinical studies in immune-poor melanoma showed that an IFN-I response induced by poly(I:C) (polyinosinic:polycytidylic acid) inhibited tumor growth and increased survival alone and in combination with anti-PD-1 mAb checkpoint blockade.¹⁸ In this model, the effectiveness of poly(I:C) was particularly reliant on interferon-gamma positive (IFN γ ⁺) CD8 T and NK cells.¹⁸ With the numerous targets and potential pathways stimulated by IFN-I along with the variations in tumor immune landscape, the mechanisms of IFN's actions could be distinct between tumor types.

IFN α has been shown to increase programmed death ligand-1 (PD-L1) and programmed cell death protein-1 (PD-1) expression on tumor and immune cell subsets.^{19,20} Induction of PD-L1 and PD-1 has led to adaptive immune resistance by promoting T cell exhaustion and immune evasion.^{19–22} This consequence may decrease the effectiveness of IFN α as a monotherapy, but in combination with immune checkpoint blockade may lead to improved therapeutic outcomes. Indeed, acquired resistance to PD-1/PD-L1 blockade is associated with loss of genes encoding IFN receptor-associated Janus kinases, JAK1 and JAK2.^{23,24} Additionally, non-responders to checkpoint inhibitors such as anti-Cytotoxic T-Lymphocyte Antigen-4 (anti-CTLA-4) possess tumors with co-deletions of IFN α and IFN β genes on chromosome 9p21 and defects in IFN γ pathway genes.²⁴ These findings highlight the potential exploitable relationship between not only PD-1/PD-L1 and IFNs, but other checkpoint molecules as well.

Understanding the relationship between IFN α and immune checkpoint inhibition is important for interpreting immunotherapy resistance and improving the treatment of UC and other solid tumors. In this study, we show that Ad-IFN α /Syn3 induces an IFN response in the bladders of human NMIBC patients with corresponding increases in T cell and checkpoint molecule expression. To elucidate the immune mechanisms underlying IFN-I's antitumor activity in UC, we utilized local injection of the synthetic dsRNA poly(I:C) into MB49 tumors in syngeneic C57BL/6 mice. Poly(I:C) is used as an IFN-I surrogate as it stimulates the IFN-I pathway. Indeed, we found that poly(I:C) induces an IFN-I response, inhibits tumor growth, and increases immune cells in murine MB49 tumors but the antitumor activity was not specifically reliant on any one immune cell type, unlike the studies performed in melanoma.¹⁸ Interestingly, however, there was an important anti-tumor role for IFN-I induced IL-6. Furthermore, poly(I:C) used in combination with anti-PD-1 mAb therapy prolonged animal survival. Combination treatment also led to decreases in tumor angiogenesis, and increases in gene expression associated with metabolism, migration, and MAPK signaling. Here our work has identified that not only does IFN-I inhibit UC tumor growth by directly decreasing angiogenesis and inducing cell death, but also through IL-6 signaling and a collaborating network of immune cells. We also show that combination IFN-I and anti-PD-1 mAb checkpoint blockade increases survival, providing preliminary justification for combination IFN-I and anti-PD-1 mAb use in NMIBC patients.

Results

Ad-IFN α Therapy in BCG-Unresponsive NMIBC Patients Induces an IFN-I Response in the Bladder and Increases Expression of T cell and Checkpoint Markers

Because our previous preclinical data and Phase I trials have provided evidence that localized, sustained IFN could be therapeutically beneficial to BCG-Unresponsive NMIBC patients,^{8,10,15} a Phase II trial with intravesical Ad-IFN α /Syn3 was conducted in 39 patients.⁹ To confirm that localized Ad-IFN α /Syn3 treatment induced a sustained IFN-I phenotype, we measured cytokine concentrations in patient urines. Ad-IFN α /Syn3 instilled on Day 1 significantly increased urine levels of IFN α 2, CXCL10 on Day 4, with additional increasing trends in TRAIL, CCL2, IL-6, and G-CSF on Day 4. Significant increases in IFN α 2, CXCL10 were still present by Day 12 (Figure 1(a)). Interestingly, the correlation of increased urinary IFN α 2 and IL-6 levels from Day4:Day1 (D4:D1) was significant for 13 patients who exhibited a complete response (CR) to Ad-IFN α /Syn3 therapy, and not significant for patients deemed “non-responders” (NR, 26 of 39 patients) (Figure 1(b)). There was also positive correlation for increased G-CSF levels in relation to increased IFN α 2 and CR at Day 4, but it did not reach statistical significance (Figure 1(b)). There was no positive correlation with any other cytokine from Day12:Day1 (D12:D1) in relation to increased IFN α 2 and CR (Supplementary Figure 1). Interestingly, there are significant positive correlations of IFN α 2 level vs. CXCL10 and TRAIL on D4:D1 for 26 of 26 patients who did not achieve CR, and IFN α 2 vs. CXCL10, CCL2, and IL-6 on D12:D1 from 24 of 26 of these patients (Supplementary Figure 1). This may be related to a prolonged inflammatory response that may have deleterious effects on the patient and tumor as noted in other tumor models,²⁵ but is an area for further investigation in NMIBC. Whole transcriptome RNAseq was conducted with matched pre-treatment and post-treatment tissue specimens from eight patients with BCG-unresponsive NMIBC, treated with Ad-IFN α /Syn3 in the Phase I trials.^{8,10} Gene expression of *PD-L1*, *CTLA-4*, and several T cell markers were markedly increased in two of eight (25%) matched tumor pairs following treatment with Ad-IFN α /Syn3 (Figure 1(c)). Less dramatic upregulation of one or more immune biomarkers was evident in four of the six additional tumors. In addition, histology sections from five of the eight tissue samples were also stained for CD3⁺ T cells. IHC analysis of these tumors showed an increase in CD3 T cells, localized in the tumor stroma, after treatment with Ad-IFN α /Syn3 in one of five samples (Figure 1(d)), and undetectable changes in the CD3⁺ populations in the other four samples (data not shown), exemplifying IFN α 's ability to enhance intratumoral T cells with variability in patients. Despite the heterogeneity of tumor response, none of the eight patients analyzed achieved CR at 12 months.

Type I IFN activation by poly(I:C) impairs MB49 bladder cancer growth

To determine how local induction of IFN-I impacts tumor growth in a murine model of bladder cancer, MB49 bladder

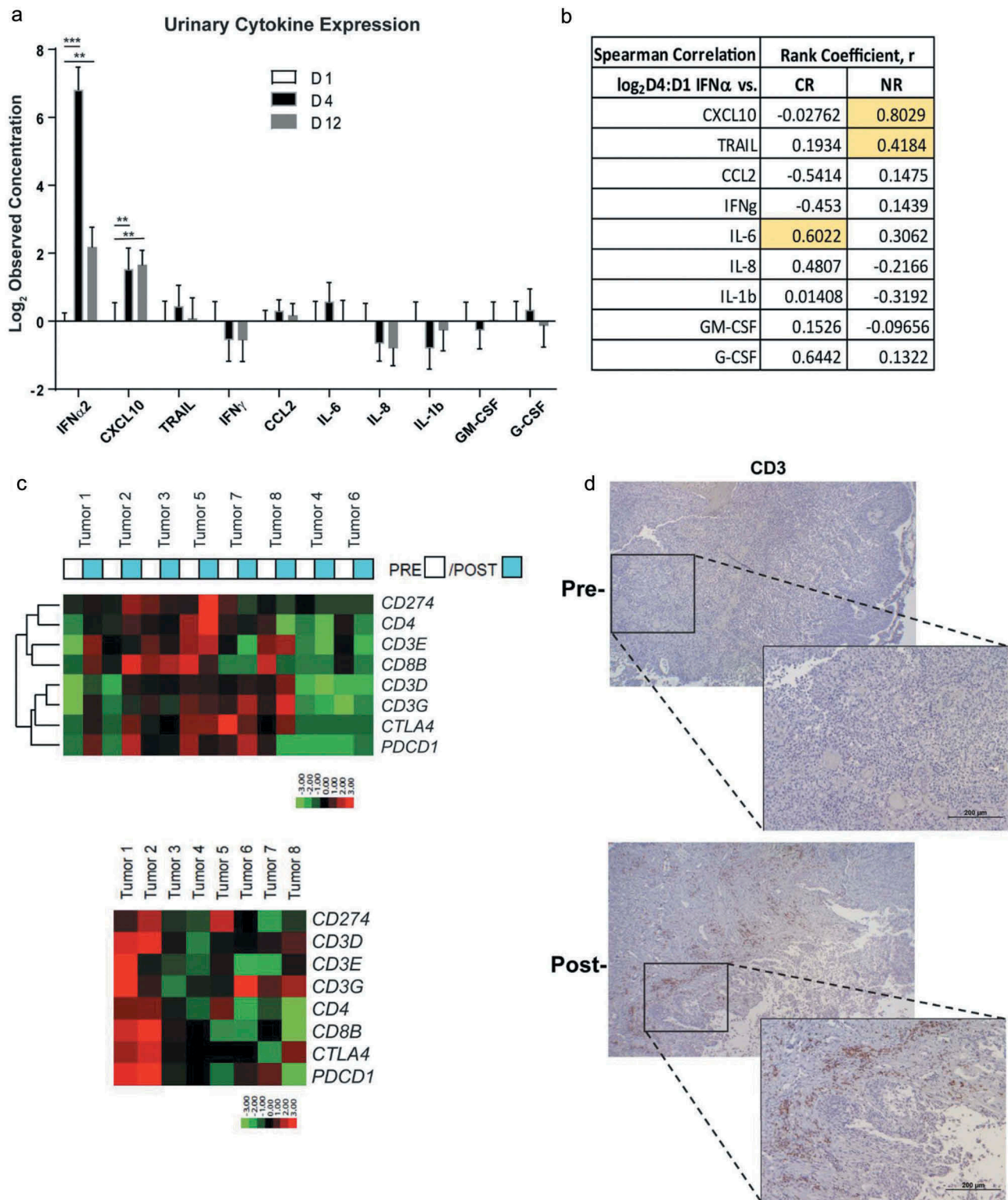


Figure 1. Effects of intravesical Ad-IFN α /Syn3 therapy on T cells and immune biomarkers in patients.

(a) \log_2 observed concentration (Day 1 pre- Ad-IFN α therapy [D1], Day 4 post-Ad-IFN α therapy [D4] or Day 12 post-[D12]) of levels for cytokines indicated. Significant p-value (one way ANOVA, multiple comparisons) $**p < 0.01$ and $***p < 0.001$ comparing D1:D4 and D1:D12 (Error bars: mean \pm SEM; $n = 39$). (b) Spearman correlation between \log_2 expression of IFN α 2 levels and respective cytokine indicated from ratio of Day 4 post-Ad-IFN α /Syn3 to Day 1 pre-treatment in 39 patient urines. Rank coefficient $r > 0.5$ indicates a positive correlation with IFN α 2. Yellow boxes indicate significant p-value (Two tailed) $*p < 0.05$, $***p < 0.001$. CR = Complete Response patients; NR = Non-Responder patients. (c) RNA from macrodissected matched tumors collected before or after Ad-IFN α therapy was analyzed by whole transcriptome RNAseq (Ion Torrent Ampliseq platform). Top panel: ratio of gene expression in post-treatment to pretreatment specimens. Note: gene expression increased significantly in two of the eight tumor pairs. Red = increased expression, green = decreased expression. Bottom panel: heat map displaying differential gene expression in each tumor pair. (d) Immunohistochemistry staining of CD3 $^+$ cells in a patient tumor (Tumor 1 (C)), pre- and 3 months post-treatment with one dose of Ad-IFN α /Syn3. Scale bar = 200 μ m.

tumor cells were implanted subcutaneously into syngeneic wild-type (WT) mice, followed by peritumoral injections of established tumors with either poly(I:C) (100 μ g) or PBS every three days; changes in tumor growth were monitored over time (Figure 2(a)). MB49 cells were chosen owing to characteristics reminiscent of non-muscle-invasive, non-metastatic UC.²⁶ Treatment with poly(I:C) delayed MB49 tumor growth and significantly improved overall survival (Figure 2(a,b)). The anti-tumor effect of poly(I:C) was mediated through IFN α signaling as poly(I:C) did not induce tumor regression in IFNAR $^{-/-}$ mice (Figure 2(c)). Poly(I:C)-mediated tumor regression is likely mediated in part through direct effects of IFN-I as murine IFN α increased MB49 cell death *in-vitro* at doses over 100 IU/mL (Figure 2(d)). For reference, one dose of poly(I:C) (100 μ g) induced an average \sim 400 pg/mL of intratumoral IFN α , and showed clearance from the serum in 24 h (Supplementary Figure 2A, B). Similar to the observed effects with Ad-IFN α /Syn3 in human urine and tumors and in immune-poor melanoma (Figure 1(a-c)),¹⁸ poly(I:C) treatment of MB49 tumors also led to an induction of IFN-I responsive genes *IRF7* and *PD-L1* compared with PBS-treated controls, as determined by RT-PCR (Figure 2(e)). Furthermore, the increase in *IRF7* expression significantly correlated with the up-regulation of *CD274* (*PD-L1*)

gene expression across all tumor samples (Figure 2(e)). These data show that poly(I:C) inhibits MB49 tumor growth and prolongs survival in an IFN α -dependent manner. These data also confirm in the MB49 model that IFN α has direct anti-tumor action, and that IFN-I induces PD-L1 expression, as previously reported.²⁰ Other murine UC cell lines BBN975, UPPL1541, and UPPL1595 were also used to evaluate the *in vivo* response to poly(I:C); however, these tumor models exhibited spontaneous regression in PBS-treated controls, or inconsistent growth patterns per replicate, and were not deemed as viable tumor growth models (Supplementary Figure 2C-E).

Poly(I:C) activates intratumoral innate and adaptive immune cells

To investigate how poly(I:C) impacts intratumoral immune responses, we examined established MB49 tumors for gene expression and immune cell infiltration 24 h after the prior treatment (day 14) with peritumoral poly(I:C) as described. Poly(I:C) significantly induced the expression of IFN-I regulated gene *CXCL10*, with other trending gene expression increases in *IRF7* and the effector cytokines *TNFA* and *PRF1* (*perforin*)

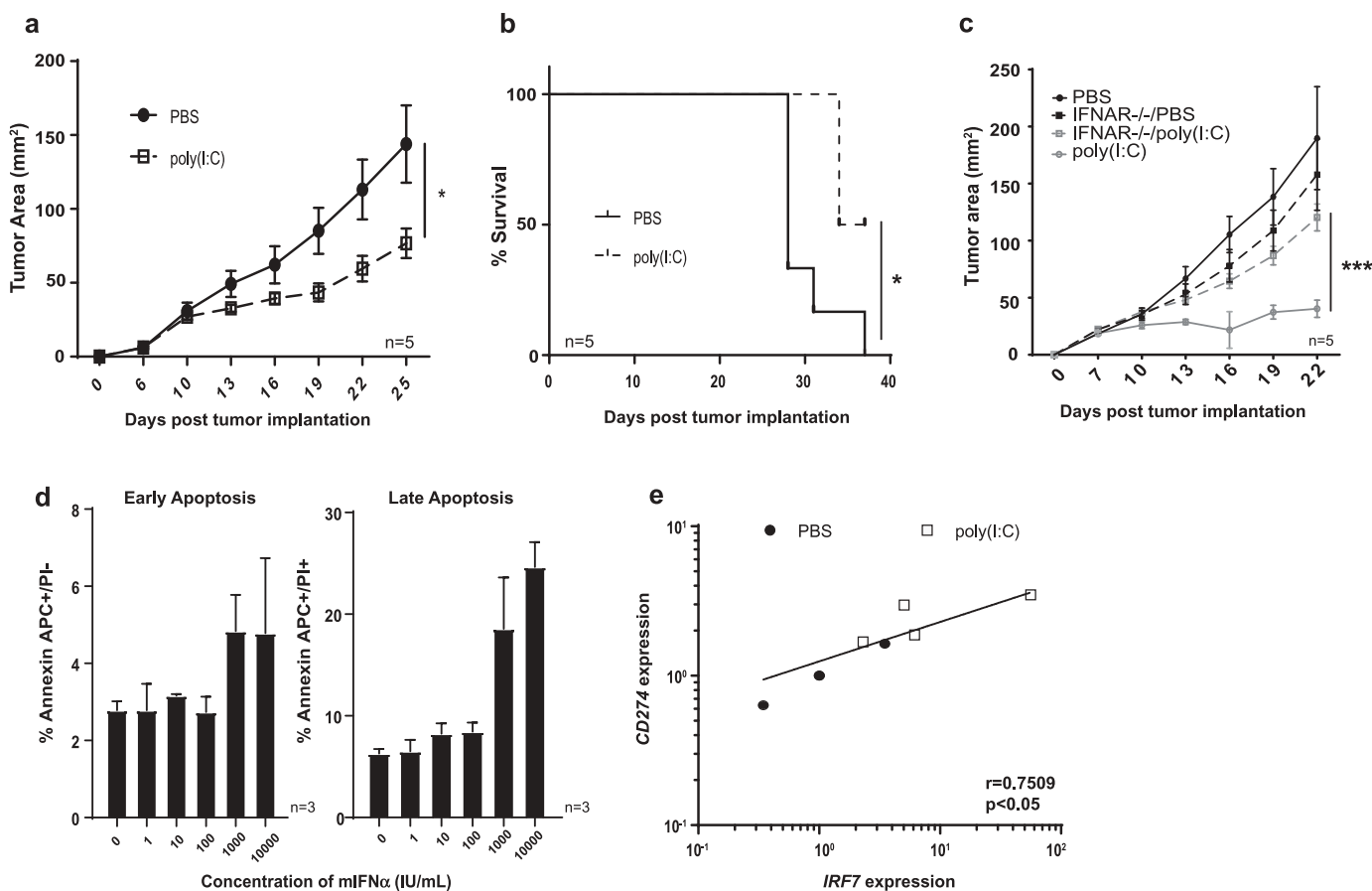


Figure 2. Poly(I:C) Treatment impairs MB49 tumor growth while upregulating PD-L1 expression on tumors.

(a) Tumor growth of subcutaneous MB49 tumors treated peritumorally with PBS (closed circles) or poly(I:C) (open square) beginning 7 days post-tumor implantation and continuing every 3 days. (b) Kaplan-Meier analysis showing survival of mice from (a). (c) MB49 tumor growth curves of poly(I:C) or PBS-treated mice in WT or interferon alpha receptor knockout (IFNAR $^{-/-}$) mice. (d) AnnexinV/PI staining for early (Annexin+PI $^{-}$) and late (Annexin+PI $^{+}$) stage cell apoptosis of MB49 cells treated *in vitro* with increasing doses of murine IFN α . (e) Correlation of relative gene expression for *CD274* and *IRF7* in control and poly(I:C)-treated MB49 samples determined by qRT-PCR. Error bars indicate mean \pm SEM; n = 5 mice per group in tumor growth/survival and n = 3 for *in vitro*. *p < 0.05, ***p < 0.001 with Student's *t* test or Log-Rank test (Kaplan-Meier).

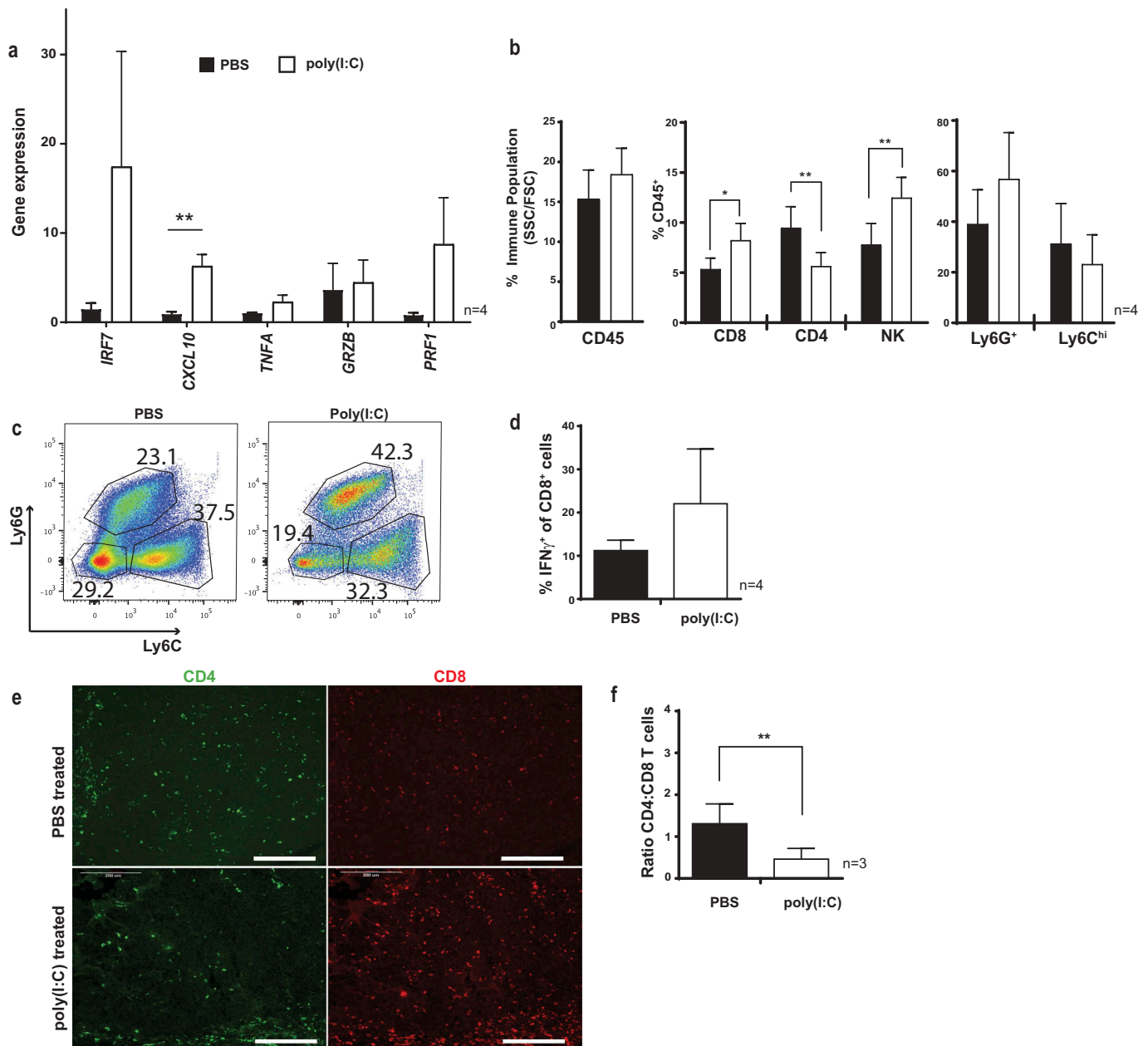


Figure 3. Induction of Type I IFN by poly(I:C) enhances immune cell infiltration and activation.

(a) Relative gene expression of immune genes from whole tumors treated with PBS or poly(I:C); Error bars indicate mean \pm SEM; $n = 4$. (b) Percentage of tumor-infiltrating immune cells in poly(I:C)-treated tumors compared to PBS-treated controls at day 14, $n = 4$. (c) Flow cytometry plot depicting frequencies of Ly6G⁺, Ly6C⁺, and Ly6G⁺Ly6C⁻ cells in a mouse from each group in (b) analysis, gated from CD45⁺CD11b⁺CD11c⁻ cells. (d) Percentage of ex-vivo CD3 stimulated IFN γ ⁺ CD8 T cells from PBS- or poly(I:C)-treated tumors after two treatments at day 11. Image representative of three tumor samples per treatment group. Scale bar = 200 μ m. (e) Immunofluorescent staining of tumor-infiltrating CD8⁺ (red) and CD4⁺ (green) cells in PBS- or poly(I:C)-treated tumors after two treatments at day 11. Image representative of three tumor samples per treatment group. Scale bar = 200 μ m. (f) Ratio of CD4:CD8 T cells calculated from tumors in (e); $n = 3$ per group. * $p < 0.05$, ** $p < 0.01$ with Student's t test.

(Figure 3(a)). We also observed a significant increase in the percentage of CD8 T cells and NK cell populations and decrease in percentage in CD4 T cells in tumor infiltrates (Figure 3(b)). Additionally, there was a consistent increase in Ly6G⁺ cells and accompanying decrease Ly6C⁺Ly6G⁻ (Ly6Chi) and Ly6C⁻Ly6G⁻ (Ly6Clo) populations (Figure 3(b,c)), demonstrating that poly(I:C) alters the composition of CD11b⁺ myeloid cell

subsets. The CD8⁺ T cells in the poly(I:C)-treated tumors showed a trend in increased expression of IFN γ (Figure 3(d)), which was not statistically significant. This increased IFN γ may be due to an exhausted CD8⁺ T cell phenotype caused by the IFN-I induced *PD-L1* expression in the tumors (Figure 2(e)). We could also observe similar effects in poly I:C-mediated changes in T cells in tumor tissue sections. After two treatments of poly(I:C) (i.e. day

11) the total numbers of intratumoral CD8⁺ T cells increased while CD4 T cells decreased (Figure 3(e)). While these changes were not statistically significant, there was a significant decrease in the ratio of CD4:CD8 T cells compared with PBS-treated control mice (Figure 3(f)). Altogether, these findings suggest poly(I:C) promotes immune cell recruitment and/or expansion.

Though inconsistent for tumor growth studies, UPPL1541 and UPPL1595 tumors were analyzed for their immune infiltration with poly(I:C) treatment as compared with PBS-treated controls. Mixed effects of poly(I:C) were observed in UPPL1541 tumors, whereby poly(I:C) increased the percentage of total intratumoral CD45⁺ cells, CD11b⁺Ly6G^{+/lo} and decreased the CD11b⁺Ly6C^{hi}Ly6G⁻ population similar to MB49, but T cells were not affected. In UPPL1595 tumors, which showed minimal growth inhibition from poly(I:C) (Supplementary Figure 2), the CD45⁺ population decreased with poly(I:C) treatment; however there were increases in the CD8 T cells, NK cells, and CD11b⁺Ly6G⁺ populations, similar to MB49 (Supplementary Figure 3A, B). The inconsistent tumor growth kinetics of both UPPL tumors despite both tumor lines exhibiting similar molecular subtypes and mutations²⁷ may be a factor in their immune infiltrate differences, and led us to believe these models needed to be further investigated before use in our study.

IL-6 is important for poly(I:C) anti-tumor efficacy, but no specific immune cell population is required

To understand the role of individual immune cell types in MB49 tumor progression and IFN-I-mediated antitumor responses, we examined tumor inhibition in mice deficient in various innate and adaptive cells. MB49 tumor growth in PBS-treated RAG^{-/-} mice was increased in compared to PBS-treated WT mice; however, tumor growth was equivalent in poly(I:C)-treated RAG^{-/-} and WT mice (Figure 4(a)). Similarly, depletion of T cell populations with anti-Thy1.2 or anti-CD8 mAbs led to increased tumor growth in PBS-treated mice, but did not affect tumor growth in poly(I:C)-treated mice (Figure 4(a)). Altogether, these data indicate that while adaptive immune cells moderate growth of MB49 tumors in untreated controls, they were not critical for the poly(I:C)-mediated antitumor response. While IFNs can stimulate NK cells and an IFN γ ⁺ NK cell antitumor response,¹⁸ in our MB49 model, depletion of NK cells led to a reduction in tumor growth (Figure 4(a)) suggesting NK cells do not play a critical role in the anti-tumor activity of poly(I:C) in the MB49 model. To address the role of neutrophilic MDSCs and monocytes/macrophages, efficacy of poly(I:C) was examined in mice depleted of Ly6G⁺ or CSFR1⁺ cells, respectively. Whereas depletion with α Ly6G mAb had no effect on tumor growth in either PBS- or poly(I:C)-treated mice, depletion of CSFR1⁺ cells led to significant tumor regression in control mice but not (poly)I:C-treated mice. These results suggest that in this tumor model, CSFR1⁺ tumor-associated macrophages, but not Ly6G⁺ cells have anti-tumor activity but are not critical to the poly(I:C)-mediated anti-tumor response. Interestingly, we observed a modest abscopal effect following the treatment of the primary MB49 tumor with poly(I:C) (Figure 4(b)) that was abrogated when mice were depleted of CD8⁺ T cells (Figure 4(c)). Collectively, these findings

suggest that T cell adaptive immunity is enhanced by poly(I:C) treatment but is not crucial for its antitumor effect.

We also examined the roles for IL-15 and inducible nitric oxide synthase (iNOS) in the IFN-I response due to the central role for IL-15 in driving IFN-mediated T cell and NK cell responses,²⁸ and the reported use of iNOS as an anti-tumor effector produced by Ly6G⁺ neutrophils.²⁹ In IL-15 receptor α deficient mice (IL15R α ^{-/-}), both PBS and poly(I:C) treatments had similar anti-tumor effects as in WT mice indicating a minimal role for IL-15 in the poly(I:C) response (Supplementary Figure 4A). Drug-mediated inhibition of iNOS by N-iminoethyl-L-lysine (L-NIL) had no effect on tumor growth when animals were treated with poly(I:C) however, in PBS-treated mice, inhibition of iNOS reduced tumor growth (Supplementary Figure 4B). Because activation of innate cells can lead to production of IL-12, a cytokine important in the Th1 immune response and IFN γ induction,^{30,31} we looked at the gene expression of both IL-12 isoforms and their heterodimeric receptor and found that poly(I:C) does significantly increase IL-12p40 and IL-12Rb1 expression within tumors (Supplementary Figure 4C). Collectively these results suggest that the regulation of IL-15 or iNOS by IFN-I are not critical to the antitumor response of poly(I:C) in this model system, but there may be a role for IL-12 influencing the IFN-I induced Th1 response.

Due to the positive correlation of IL-6 with IFN α and patient response (Figure 1), we investigated the effect of IL-6 in MB49 tumor growth. The anti-tumor benefit of poly(I:C) was significantly inhibited in IL-6 knockout mice (IL-6KO), and survival of poly(I:C) treated IL-6KO mice was also significantly decreased as compared to poly(I:C) treated WT mice. (Figure 4(d,e)). In addition, poly(I:C) upregulated IL-6 protein as poly(I:C)-treated MB49 tumors had higher levels of IL-6 per mg of tumor as compared to PBS-treated controls (Figure 4(f)). As in earlier experiments (Figure 3(b,c)), poly(I:C) altered the myeloid cell landscape by significantly increasing the frequency of Ly6G⁺ cells and decreasing Ly6Chi and Ly6Clo cells within the tumors (Figure 4(g)). Interestingly, these changes in the myeloid cell landscape did not occur in tumors present in the IL-6KO (Figure 4(g)). Among tumor lymphocytes, the changes in NK and T cells observed in poly(I:C)-treated tumors in WT mice were still intact in IL-6KO mice, though the poly(I:C)-mediated increase in CD8 and decrease in CD4 T cells was slightly impaired in IL-6KO (Figure 4(h)). We also examined additional parameters of lymphocyte activation in the poly(I:C)-treated WT and IL-6KO mice. Within secondary lymphoid tissues, poly(I:C) increased the frequency of Ki-67⁺ NK cells and CD8 T cells in spleens and draining lymph nodes (dLN) but not in tumors, which was abrogated in IL-6KO mice (Supplementary Figure 5A,B, data not shown). Similarly, there was an increased frequency of Granzyme B⁺ CD8 T cells in dLN with poly(I:C) treatment that was impaired in IL-6KO mice (Supplementary Figure 5C). Overall, the anti-tumor response elicited by IFN-I likely represents the collective activity of multiple cellular components of the adaptive and innate immune response pathways.

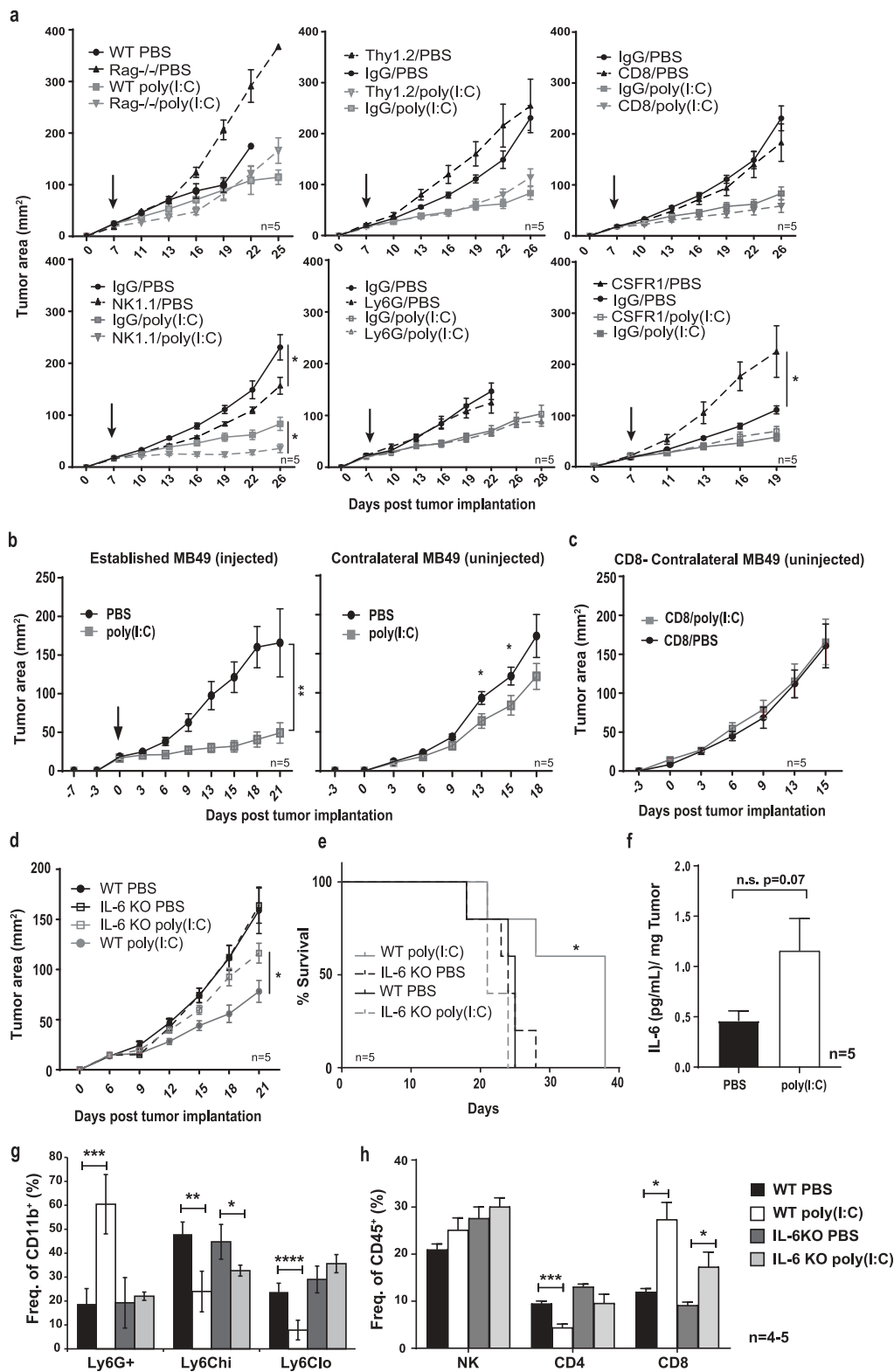


Figure 4. Anti-tumor efficacy of poly(I:C) relies on IL-6 signaling and multiple immune subtypes.

(a) Growth of MB49 tumors treated peritumorally with PBS or poly(I:C) in RAG-/- mice or WT mice depleted of specific immune cell populations with the indicated Ab or given control Ig. Anti-Thy1.2 mAb was used to deplete T cells and anti-CSFR1 mAb was used to deplete monocytes and macrophages; $n = 5$ per group. (b) Tumor growth of primary and secondary MB49 tumors in WT mice. Primary ("Established") tumors were treated peritumorally with either PBS or poly(I:C) beginning 7 days post-implantation. Secondary ("Contralateral") tumors were implanted 4 days after the primary tumors. Arrow indicates the beginning of treatment. (c) Tumor growth of the contralateral tumor similar to (b) in CD8 depleted mice. (d) Growth of MB49 tumors treated peritumorally with PBS or poly(I:C) in IL-6 knockout (IL-6KO) or WT mice. (e) Kaplan-Meier analysis of survival of mice from (d); $n = 5$. (f) Average concentration of IL-6 (pg/mL) per tumor weight (mg) in MB49 tumors from Day 14 tumors treated with either poly(I:C) or PBS; $n = 5$ per group. (g) Frequency (percentage) of Ly6G⁺, Ly6Chi, and Ly6Clo cells and (h) frequency of NK, CD4, CD8 T cells from MB49 tumors of WT and IL-6KO mice treated with PBS or poly(I:C) among gated CD45⁺CD11b⁺ cells and CD45⁺ cells, respectively; $n = 5$. Error bars indicate mean \pm SEM; * $p < 0.05$, ** $p < 0.01$, *** $p < 0.001$, **** $p < 0.0001$ with Student's *t* test.

Combination treatment with Anti-PD-1 mAb and poly(I:C) reduces tumor burden and prolongs survival

Given that IFN-I signaling induces expression of checkpoint markers such as PD-L1 (Figures 1 and 2) which may lead to decreased effector T cell function,¹⁹⁻²² we reasoned that therapeutic blockade of the PD-1/PD-L1 pathway could further enhance the anti-tumor efficacy of poly(I:C). Subcutaneous MB49 tumor-bearing mice were treated with poly(I:C) and a PD-1-blocking mAb either as monotherapies or in combination (Figure 5(a)). Tumor growth was measured overtime until mice became moribund. Treatment with both single-agent poly(I:C) and combination therapy [poly(I:C) with anti-PD-1 mAb] significantly repressed tumor growth compared with anti-PD-1 mAb alone and IgG/PBS-treated controls (Figure 5(b)). However, we observed no significant difference in tumor growth inhibition between poly(I:C) monotherapy and combination therapy. Nonetheless, combination therapy significantly prolonged survival compared with poly(I:C) alone (Figure 5(c)) demonstrating IFN-I can work with checkpoint blockade for enhanced efficacy.

Combination Treatment Induces MAPK Signaling, Metabolic Pathways, and Reorganization of Tumor Microenvironment

To examine potential molecular changes between treatment groups, comprehensive gene expression analysis was performed via RNA sequencing and GSEA on total mRNA collected from day 17 tumors treated with PBS, poly(I:C), anti-PD-1 mAb, or in combination. GSEA of the RNAseq data from the poly(I:C), anti-PD-1 mAb, and the combination showed enrichment in viral stress response, IFN signaling, cytokine signaling pathways, and innate immune response in comparison to control tumors (Table 1). However, the single agent anti-PD-1 mAb as well as the combination treatment also enriched pathways promoting cell migration, differentiation, proliferation, and survival through MAPK, MEK/ERK and AKT signaling (Table 1). Combination treatment up-regulated additional pathways related to collagen formation, extracellular matrix formation, and cell-cell signaling (Table 1). Comparing the poly(I:C) and combination treated groups to each other, metabolic pathways for glucokinase regulation and fatty acid oxidation (FAO) and synthesis were enriched in the combination group (data not shown).

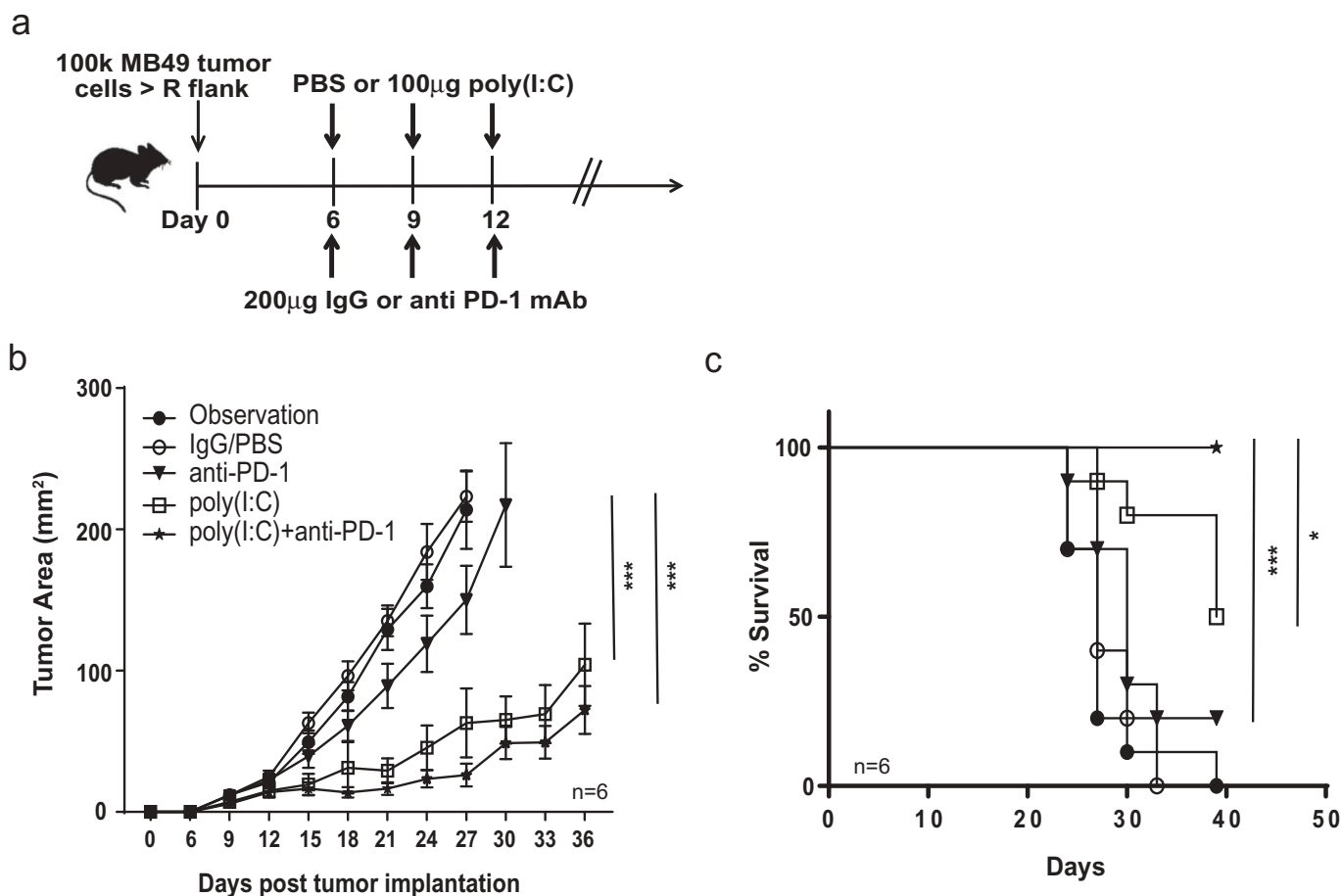


Figure 5: Blockade of PD-1/PD-L1 pathway reduces tumor burden and prolongs survival in poly(I:C) treated mice.

(a) Experimental strategy for combination therapy for s.c. engrafted MB49 tumors for peritumoral poly(I:C) and anti-PD-1 mAb (i.p.). (b) Averaged tumor growth of mice treated with either single agent poly(I:C) or anti-PD-1 mAb, poly(I:C) plus anti-PD-1 mAb, or control IgG plus PBS or control observation. (c) Kaplan-Meier analysis of survival of mice from (b). Error bars indicate mean ± SEM, n = 10; *p < 0.05, **p < 0.01, ***p < 0.001 with Student's *t* test or Log-Rank test; Graphs representative of three separate trials.

Table 1. Summary of the reactome gene sets enriched in treatment groups: name, process category, description, number of genes involved, NES.

Treatment	Reactome Name	Process category	Description	Number of genes	NES*	
Poly(I:C)	Activation of genes by ATF4	Signaling	Transcription factor; response to ER stress, PERK signaling	21	1.89	
	PERK regulated gene expression	Signaling	Integrated stress response and protein folding	24	1.79	
	Interferon γ signaling	Immune	Type II IFN signaling	42	1.75	
	Toll receptor cascades	Immune	TLR stimulated immune signaling	109	1.65	
	Class I MHC mediated antigen processing/presentation	Immune	Innate and adaptive immune recognition of antigen	221	1.59	
	TRAF6 mediated IRF7 activation	Immune	Viral, IFN response	20	1.58	
	Trans golgi network vesicle budding	Pathway	Secretory pathway for synthesized proteins	52	1.58	
	ER Phagosome pathway	Pathway	Cell death pathway	53	1.56	
	Latent infection of homo sapiens with mycobacterium tuberculosis	Immune	Innate immune effectors	30	1.55	
	Antigen processing cross presentation	Immune	Antigen presentation	65	1.55	
	Antigen presentation, folding, assembly, and peptide loading of Class I MHC	Immune	Antigen presentation	15	1.54	
	Innate immune system	Immune	Innate immune signaling	201	1.68/1.58	
	IL-1 signaling	Immune	Damage associated molecular pattern (DAMP), inflammatory signaling	37	1.63/1.68	
	*	Nucleotide binding domain Leucine rich repeat containing receptor NLR signaling pathways	Signaling	NOD-like receptor signaling, viral response	42	1.59/1.54
NOD1/2 signaling pathway		Immune	NOD-like receptors for antigen recognition, inflammatory signaling	29	1.58/1.71	
Interferon signaling		Immune	Interferon signaling	121	1.88/1.77/1.7	
Interferon $\alpha\beta$ signaling		Immune	Type I IFN signaling	43	1.77/1.65/1.62	
Cytokine signaling in Immune system		Immune	Cytokine signaling	224	1.75/1.77/1.52	
Antiviral mechanism by IFN stimulated genes		Immune	Antiviral stress response through IFN	62	1.72/1.99/1.97	
Negative regulators of RIG-I MDA5 signaling		Immune	Viral recognition receptor sensing	28	1.69/1.58/1.55	
Interaction between L1 and ankyrins		Development	Cell adhesion molecules	20	1.67	
Signaling by ILS		Immune	Inflammatory signaling	102	1.57	
SEMA4D in semaphorin signaling		Signaling	CD100 binding to CD72 to activate immune cells	28	1.55	
Myogenesis		Development	Muscle differentiation	26	1.54	
Platelet aggregation plug formation		Development	Muscle differentiation	35	1.54	
JNK, C-JUN Kinases phosphorylation and activation mediated by activated human TAK1		Signaling	JNK signaling; stress response, IRF3, T cell differentiation and apoptosis	16	1.53	
#		MAP Kinase activation in TLR cascade	Signaling	MAPK signaling in stress response	49	1.52
	SEMA4D induced cell migration and growth cone collapse	Signaling	CD100 binding activation, immune activation by CD72	24	1.64/1.63	
	SHC1 events in ERBB4 signaling	Signaling	MAPK signaling, cell migration, survival, differentiation	19	1.6/1.63	
	MAPK targets/Nuclear events mediated by MAP Kinases	Signaling	Proliferation, differentiation, survival	30	1.56/1.45	
	Signaling by PDGF	Signaling	Angiogenesis, proliferation, migration	115	1.52/1.45	
	Pre notch processing in golgi	Signaling	Maturation of notch receptor	16	1.71	
	Poly(I:C) + α -PD-1 mAb	Muscle contraction	Development	Muscle contraction	46	1.56
		Activation of chaperone genes by XBP1S	Signaling	Cellular response to ER stress, UPR	41	1.55
		Collagen formation	Development	Collagen formation	53	1.54
		Extracellular matrix organization	Development	Extracellular matrix organization	76	1.54
		Gap junction trafficking	Signaling	Cell-cell communication	24	1.52
		Chondroitin sulfate dermatan sulfate metabolism	Metabolic	Glycosaminoglycan/proteoglycan; anti-inflammatory	47	1.5
		Chondroitin sulfate biosynthesis	Metabolic	proteoglycan; anti-inflammatory	19	1.5
		ERK/MAPK targets	Survival	proliferation, differentiation, survival	21	1.47
Circadian clock		Metabolic	Circadian rhythm, metabolic pathways	49	1.46	
Gap junction assembly		Signaling	Cell-cell communication	16	1.45	

* Pathways are up-regulated in both poly(I:C) and anti-PD-1 treated groups.
Pathways are up-regulated in both anti-PD-1 and combination poly(I:C)+anti-PD-1 treated groups.
+ Pathways are up-regulated in poly(I:C), anti-PD-1, and combination treated groups.
* Normalized enrichment score (NES); up-regulated pathways defined as (NES) > 0
* Pathways are up-regulated in both poly(I:C) and anti-PD-1 treated groups.
Pathways are up-regulated in both anti-PD-1 and combination poly(I:C)+anti-PD-1 treated groups.
+ Pathways are up-regulated in poly(I:C), anti-PD-1, and combination treated groups.
* Normalized enrichment score (NES); up-regulated pathways defined as (NES) > 0

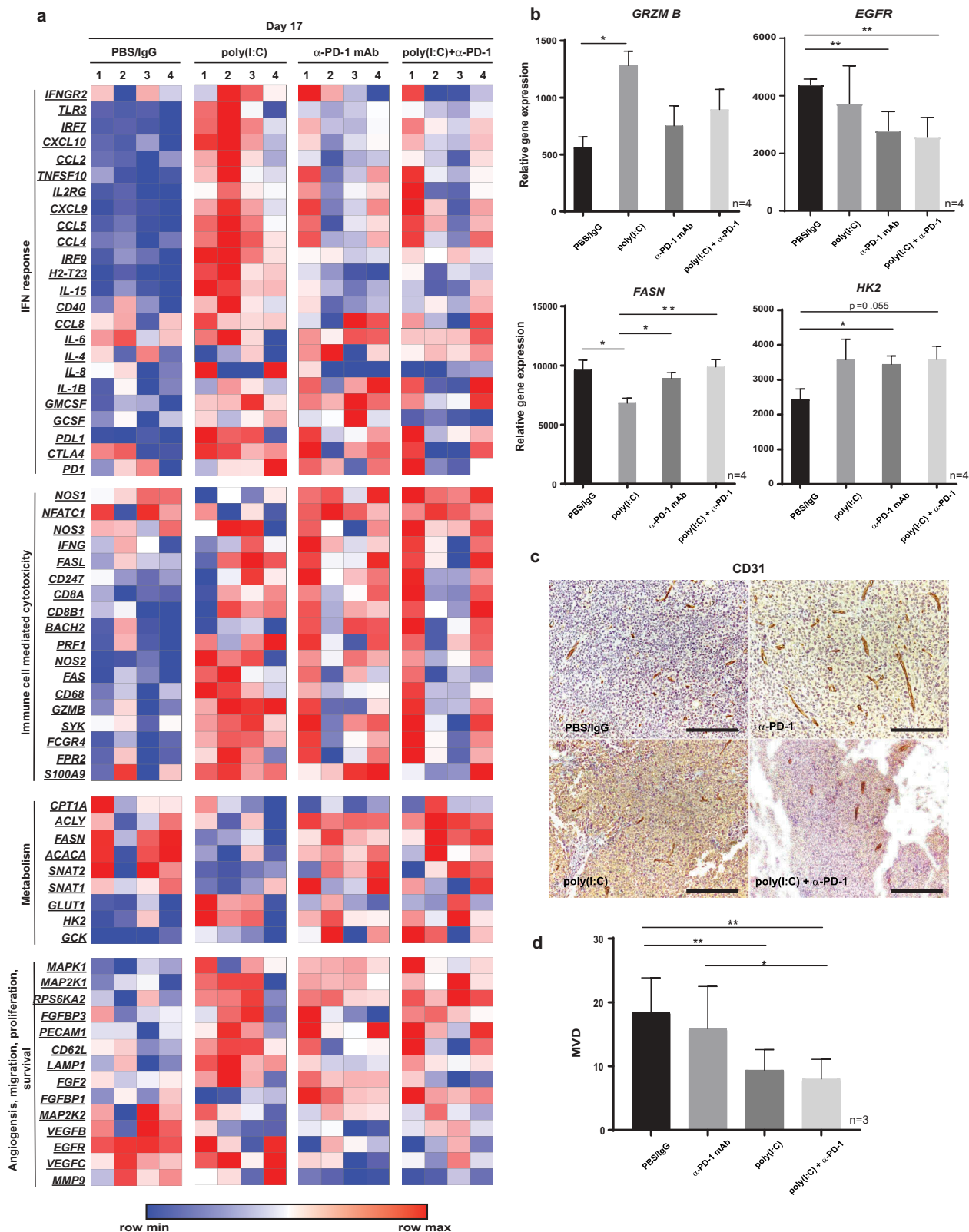


Figure 6: Poly(I:C) and anti-PD-1 mAb combination therapy promotes gene expression associated with survival, metabolism, and Th-1 type anti-tumor immunity and decreases angiogenesis.

(a) Heatmap illustrating normalized (\log_2) gene expression patterns from MB49 whole tumor lysates treated with either PBS+IgG Ab, poly(I:C), anti-PD-1 mAb, or poly(I:C)+anti-PD-1 mAb; RNA was isolated from tumors 17 days post-implantation (four treatments) (Figure 5a). Each column represents one mouse. (b) Average relative gene expression of indicated genes associated with effector function, fatty acid oxidative metabolism, glycolysis, and AKT, MEK/ERK pathway from the four treatment arms ($n = 4$ per group). (c) IHC staining for CD31 (PECAM-1) in end point tumors from 38 days post-implantation (11 treatments); Scale bar = 100 μ m. Image is representative of three tumors per treatment group. (d) Quantified microvessel density (MVD) averaged from IHC CD31-stained tumors (c) ($n = 3$ per group). All values normalized by DeSeq and \log_2 transformed (heatmap). Error bars indicate mean \pm SEM, $n = 4$ per group. * $p < 0.05$, ** $p < 0.01$ with Student's t test.

Looking more closely at effects on individual genes, we found numerous genes related to IFN pathway signaling (Figure 6(a)), as well as adaptive and innate effector cell cytotoxicity such as *Granzyme B* (*GZMB*) were significantly increased in the poly(I:C) treated group, and more modestly increased in the anti-PD-1 mAb and combination treated groups, in comparison to control IgG/PBS treated tumors (Figure 6(a,b)). As expected, there were also increases in gene expression for immune suppressive molecules in poly(I:C), anti-PD-1 mAb, and combination treated mice, including *ARG1* and *ARG2* (*Arginase 1* and *2*), *IDO*, and *CD274* (*PD-L1*) (data not shown). Exploring the GSEA-identified upregulated metabolic pathways, we found poly(I:C) induced expression of glucose transporter *GLUT1*, and all treatment groups increased expression of glycolysis enzymes *HK2* and *GCK* in comparison to PBS/IgG control (Figure 6(a, b)). Interestingly, while poly(I:C) decreased tumor expression of genes related to fatty acid catabolism and synthesis such as *FASN*, *ACACA*, and *ACLY* in comparison to PBS control, anti-PD-1 mAb and combination treatment significantly rescued their expression (Figure 6(a,b)). We also observed increased *MAPK* signaling genes in all treated groups in comparison to control, and decreased expression of *VEGF*, *MMP9*, and *EGFR*. Similar trends in gene expression were also observed in the eight matched pre- and post-Ad-IFN α /Syn3 treated patient tumor specimens from Figure 1(c) (Supplementary Figure 6). Many of the IFN response and immune cell-mediated cytotoxicity genes such as *CXCL10*, *CCL5*, *CCL4*, *CCL2*, *PRF1*, *CD8A*, and *NFATC1* were induced in at least four of the eight patient samples post-Ad-IFN α . Interestingly, four of eight patients also had an increase in *IL-6* gene expression. There was also similar decreased tumor expression of genes related to fatty acid catabolism (*FASN*, *ACLY*, *ACACA*), amino acid transport, and *VEGFA* post-treatment. However, none of these eight patients were deemed as clinical responders (CR). To further investigate the decreased expression of angiogenesis markers seen in the RNAseq of MB49 tumors treated with poly(I:C), anti-PD-1 mAb, or combination, we performed IHC staining of CD31 on tumors from each treatment group taken at their end point (day 38) (Figure 6(c)). Poly(I:C) alone and in combination with anti-PD-1 mAb significantly decreased microvessel density (MVD) compared to control PBS/IgG treated tumors by ~50% (Figure 6(d)). Thus, while IFN-I has significant anti-tumor action, combination therapy with checkpoint blockade activates additional pathways regulating the increased stromal influx and reorganization of ECM, inhibition of angiogenesis, glycolysis and fatty acid catabolism, and increased *MAPK/ERK/AKT* signaling that may be related to prolonged survival.

Discussion

In this study, we examined the immune mechanisms behind IFN-I-mediated anti-tumor responses in human patients with UC and in a murine model of UC. We also tested if the

combination of IFN-I with anti-PD-1 mAb checkpoint blockade provides additional efficacy. We found that IFN-I induction by poly(I:C) in MB49 tumors inhibits tumor growth, increases longevity, and activates both the innate and adaptive immune systems. The poly(I:C) mediated tumor inhibition was also dependent on functioning IL-6 signaling, mirroring a positive correlation of IL-6 urinary cytokine expression and patient response (CR) to Ad-IFN α /Syn3. Combination therapy with anti-PD-1 mAb significantly prolonged survival of mice compared to control and single agent therapies, and was associated with inhibition of angiogenesis and enrichment of glycolysis and fatty acid synthesis gene expression, and extracellular matrix organization and *MAPK/ERK/AKT* signaling pathways. Altogether, these findings suggest IFN-I's immune-driven antitumor response in UC is mediated by IL-6 and a collaboration of immune cells, and its use in combination with checkpoint blockade therapy can increase clinical benefit.

Treatment of MB49 and UPPL tumors with poly(I:C) resulted in an IFN-I induced infiltration of highly diverse immune populations representing a multifaceted pro-inflammatory anti-tumor phenotype, contrary to the defined dependence of tumor-inhibitory poly(I:C) on specific immune subsets in studies performed in melanoma.¹⁸ Previous studies in experimental bladder cancer have focused on the necessity of the T cell infiltration for an anti-tumor response, and thus have relied on T cell checkpoint targeted immunotherapy.^{26,32,33} However, the importance of both lymphoid and myeloid cell types in the anti-tumor response in our MB49 studies indicates that focusing on a single subset of effector cells may limit the insights to be gained. We also found an important role for IL-6 signaling in the type I IFN-driven MB49 tumor inhibition as well as in patients treated with Ad-IFN α /Syn3. Pro-inflammatory IL-6 has been shown to have a dichotic role in both cancer as well as autoimmune diseases, providing an activation signal to immune cells that left unchecked has the potential to produce deleterious effects.³⁴ The potential link of IL-6 to type I IFN-driven anti-tumor responses in both murine models and in patients sparks the need for further investigation of the role of this cytokine in IFN-I treated bladder cancer.

We found IFN-I pleiotropically affects multiple immune cell types, as well as directly inhibit tumor growth by decreasing tumor vasculature, similar to our prior IFN gene therapy work.¹² Angiogenesis has long been recognized as a major hallmark of cancer progression and its induction can lead to tumor invasion. Recent reports show that antiangiogenic therapy, such as VEGF/VEGFR2 inhibitors, can up-regulate PD-L1 mediated immunosuppression.³⁵ The use of antiangiogenic therapy combined with immune checkpoint blockade promotes higher lymphocyte infiltration and activity in several tumor models.³⁵ This concept is currently being investigated in clinical trials for multiple cancers. As we have seen here, combination IFN-I with anti-PD-1 mAb effectively decreases angiogenic gene regulators and reduces MVD, thus making it a prime candidate for inhibition of this hallmark pathway.

Here we show that combination treatment of MB49 tumors with poly(I:C) and anti-PD-1 mAb increases the survival of mice in comparison to either agent alone, however there is no significant difference in tumor size between single

agent poly(I:C) and combination treatment. Overstimulation of inflammatory pathways has been shown to produce a “cytokine storm” that can result in significant pathology and ultimately death.^{36,37} In a model of viral infection and poly(I:C), mice lacking an adaptive immune response (nude and Rag-/- mice) had higher mortality rates after virus/poly(I:C) dosage due to higher abundances of proinflammatory cytokines TNF and IFN γ in the serum days after infection compared to WT mice.³⁸ Addition of T cells to the non-T cell, TLR3-stimulated system efficiently prevented this cytokine surge, suggesting that active T cell monitoring is necessary to temper an innate response. One hypothesis for why combination treated mice had improved survival over poly(I:C) alone is that the addition of anti-PD-1 mAb is able to reactivate T cells that have become exhausted from IFN-I stimulated PD-L1 expression, which results in tempering of the innate cytokine response invoked by IFN-I signaling. This warrants future analysis in the MB49 model.

GSEA and RNaseq analysis of MB49 tumors treated with either single agent poly(I:C), anti-PD-1 mAb alone, or combination therapy showed anticipated enrichment in genes and pathways related to IFN induction, viral stress response, cytokine production and innate immune activation, as well as *MAPK* and *ERK* signaling in comparison to PBS-treated control tumors. MAPK/ERK signaling traditionally is associated with cell survival, proliferation, and differentiation. However, there is evidence that ERK signaling has pro-apoptotic functions in response to damage stimuli,³⁹ and this mechanism may add to the immune component of the IFN-I anti-tumor response, providing further survival benefit demonstrated in our study.

Previously published studies identified that blockade of the PD-1/PD-L1 axis reverses T cell exhaustion, re-inducing glycolysis and anabolic metabolism to produce a more active state.^{40,41} In our work, we see that poly(I:C), anti-PD-1 mAb, and combination treated groups have increased levels of enzymes involved in glycolysis and the TCA cycle. Interestingly, we also found in comparison to poly(I:C) treatment alone, the addition of anti-PD-1 mAb enriched for extracellular matrix reorganization, collagen formation, and increased genes related to FAO and fatty acid synthesis such as *FASN*, *ACLY*, and *ACACA*. Increasing mitochondrial FAO metabolism in T cells has been shown to favor the formation of long-lived memory T cells.^{42,43} However, the whole tumor RNA analyzed here is likely more reflective of the tumor genome than the immune microenvironment. Since and fatty acid synthesis and glycolysis are necessary for cellular growth and proliferation,⁴⁴ our analysis suggests that combination treated tumors are upregulating pathways of proliferation in the tumor cells while simultaneously inhibiting tumor growth. Upregulation of expression of genes involved in ECM remodeling and mesenchymal transition has been shown to be a marker of resistance to anti-PD-1 therapy (innate anti-PD-1 resistance, IPRES).⁴⁵ The possibility of combination therapy upregulating mechanisms of resistance pathways will need to be further explored in our model.

Recent US Food and Drug Administration approval of atezolizumab (anti-PD-L1mAb) and nivolumab (anti-PD-1mAb) for treatment of metastatic urothelial carcinoma⁴⁶

has brought into question the role of immune therapy earlier in the treatment of UC. Our analysis of patients who have undergone Ad-IFN α /Syn3 (Instiladrin) therapy showed upregulation of cytokines key for immune infiltration, T cell markers, and *PD-L1* (and *CTLA-4*) immune evasion markers, suggesting that these patients may be prime candidates for PD-1 blockade in addition to their gene therapy. Our studies in the MB49 model of UC likewise showed upregulation of cytokines, immune cells, and immune evasion markers after poly(I:C) (IFN-I) treatment making it a relevant preclinical model for comparison to patients. Our observation that combination treatment with poly(I:C) and anti-PD-1mAb prolonged survival of mice in a model reminiscent of invasive bladder carcinoma corresponds to results seen in immune-poor melanomas.¹⁸ It also highlights the importance of IFN therapy and the immune inhibitory PD-L1/PD-1 pathway *in vivo*.

In summary, our group’s gene therapy work with Ad-IFN α /Syn3 instillations utilizes the effectiveness of type I IFN to stimulate both the innate and adaptive immune cell subsets locally and sustainably. The improved survival we found with poly(I:C) treatment in combination with anti-PD-1mAb therapy demonstrates the utility of targeting multiple cell types and signaling pathways to improve therapeutic outcome. Our results provide a preclinical conceptual example for using type I IFN activation to increase the therapeutic benefit of PD-1 blockade for bladder cancer patients, as well as a rationale for pursuing further studies in NMIBC to optimize a treatment protocol. Due to recent work indicating that MB49 UC cells are more mesenchymal-like than urothelial-like cells,²⁷ we are in the process of optimizing the N-butyl-N-(4-hydroxybutyl)-nitrosamine (BBN) and hRAS murine NMIBC models⁴⁷ to aid in understanding the mechanism(s) of Instiladrin’s antitumor activity. These models will allow for testing of intravesical therapy with murine adenoviral IFN α vectors in NMIBC-like pathologies, and determining if similar immune mechanisms are active with intravesical gene therapy. These studies will be done in preparation for a clinical trial combining Instiladrin with a checkpoint inhibitor.

Materials and methods

Patient samples

Patient specimens utilized in this study were collected from previous Phase I, Phase Ib, and Phase II clinical trials with adenoviral interferon- α 2b formulated with Syn3 (Ad-IFN α /Syn3) with patient eligibility, treatment, and specimen collection approved by the University of Texas MD Anderson Cancer Center institutional review board.^{8–10}

Mice

Wild-type male C57BL/6J mice, IL-6KO mice, and RAG-/- mice were purchased from The Jackson Laboratory (Bar Harbor, ME). All gene-deficient mice used are on the C57BL/6 background. IFNAR-/-⁴⁸ were provided by Dr. Paul W. Dempsey (Department of Microbiology and

Molecular Genetics, University of California, Los Angeles) and Dr. Tadatsugu Taniguchi (Department of Immunology, Tokyo University, Japan) to Dr. W. Overwijk and crossed to the C56BL/6 background. IL15R α -/- mice⁴⁹ were originally generated by and obtained from Dr. Averil Ma through Dr. Leo Lefrancois and crossed to the C57BL/6 background. All animal experiments were performed according to the institutional guidelines for the care and use of laboratory animals.

Cell lines and treatment in vitro

MB49-GFP/luciferase murine bladder cancer cells were generously donated by Dr. Robert Svatek (the University of Texas Health San Antonio). Cells were grown in culture in modified Eagle medium containing 10% fetal bovine serum and 1% penicillin/streptomycin. MB49 bladder cancer cells were seeded in six-well plates and treated with 0–10,000 IU/mL recombinant murine IFN α (PBL Assay Science, Piscataway, NJ). After 24 h of stimulation, cell death and apoptosis were analyzed by a combined PI/Annexin V (APC) assay (Invitrogen [Thermo Fisher Scientific], Carlsbad, CA), and analyzed by flow cytometry whereby early apoptosis (Annexin⁺PI⁻) and late apoptosis (Annexin⁺PI⁺) were quantified (n = 2 biological replicates). UPPL1541 and UPPL1595 cell lines are established from a spontaneous primary bladder tumor in an Uroplakin-Cre driven PTEN/P53 knockout genetically engineered mouse model and were generously provided by Dr. William Kim (UNC Chapel Hill).

Tumor transplantation

Mice were injected subcutaneously into the right flank with 1×10^5 MB49 bladder cancer cells (1×10^6 or 1×10^7 for UPPL1595 and UPPL1541, respectively). For analysis of abscopal effect, following primary tumor injection of MB49 on right flank, a secondary tumor (1×10^5 MB49 cells) was injected in the left flank 4 days later. Tumor development was monitored by palpation and fluorescent imaging with the IVIS Spectrum In Vivo Imaging System and Living Image software (PerkinElmer, Waltham, MA). Mice were randomized into treatment groups on the basis of fluorescent intensity and palpated tumor size at day 6 after implantation. From day 6 on, tumor size was measured every 3 days by caliper and was recorded as Area [L \times W] in millimeters. Mice with tumors exceeding 20 mm in diameter or with large ulcerations were deemed moribund and euthanized. Each point on tumor growth graphs reflects the average area of the total starting number of mice per treatment group; graph lines are stopped when multiple mice in a group are euthanized. Experiments were performed in groups of five or more mice and repeated at least twice.

Treatment of mouse tumors and depletions

When transplanted bladder tumors became palpable, poly(I:C) (100 μ g; Invivogen, San Diego, CA) was injected peritumorally beginning on Day 6 or 7 and continued every 3 days until mice were deemed moribund, or for tumor analysis after a total of

two, three, or four treatments as denoted in Figures 2–5. Therapeutic blockade of PD-1 was performed using rat anti-mouse PD-1 mAb (200 μ g, i.p., clone RMP1-14; BioXcell, West Lebanon, NH) or control-rat IgG mAb (200 μ g, i.p.; Jackson ImmunoResearch Laboratories Inc., West Grove, PA) every 3 days in conjunction with poly(I:C) treatment. Antibody-mediated depletion of T cells or natural killer cells was induced with rat anti-mouse Thy1.2 mAb (300 μ g, i.p. clone 30H12; BioXcell), rat anti-mouse CD8 mAb (300 μ g, i.p. clone 2.43; BioXcell), or rat anti-mouse Nk1.1 mAb (300 μ g, i.p. clone PH136; BioXcell) delivered two times, 1 week apart. Ly6G and CSFR1 mAbs (400 μ g, i.p. clones 1A8 and AFS98, respectively; BioXcell) were given three times a week until mouse morbidity. Greater than 85% depletions of target cells were confirmed by flow cytometry of peripheral blood samples taken 1–2 days after Ab treatment. Efficiency of cell depletions is represented in Supplementary Figure 7. All treatments and depletions were performed in Wild-type male C57BL/6J mice, male IL-6KO mice (B6.129S2-Il6^{tm1Kopf}/J), and male RAG-/- (B6.129S7-Rag1^{tm1Mom}/J) mice (The Jackson Laboratory; Bar Harbor, ME).

T cell stimulation

For intracellular IFN γ staining, MB49 tumor-infiltrating immune cells were isolated by Percoll gradient and plated into six-well plates coated with anti-CD3 antibody, incubated in RPMI with 10% fetal bovine serum with protein transport inhibitors GolgiStop and GolgiPlug (2 μ g/mL; BD Biosciences, San Jose, CA) for 5 h (n = 4). After incubation, cells were stained for surface markers and then fixed and permeabilized prior to staining for intracellular proteins.

Murine cytokine analysis

Murine cytokines were measured by ELISA: IFN α (PBL VeriKine Mouse Interferon Alpha ELISA kit, 42120-1; Piscataway, NJ) and IL-6 (R&D Mouse IL-6 Quantikine ELISA Kit, M6000B; Minneapolis, MN). Samples were run in duplicate and ELISA was performed according to manufacturer instructions. Plates were read on Molecular Devices Spectra Max Plus384 plate reader.

Immunohistochemistry and immunofluorescence staining

Mouse tumors were fixed in 10% phosphate-buffered formalin, embedded in paraffin, and sectioned by the Research Histology Core Laboratory at The University of Texas MD Anderson Cancer Center. Patient tumors were isolated and processed according to the phase I trial protocol^{8,10} and obtained from MD Anderson. Immunohistochemistry was performed with either rat anti-mouse CD31 mAb (SZ31, Dianova, Hamburg, Germany) or rabbit anti-human CD3 pAb (A0452, Dako [Agilent], Santa Clara, CA) followed by rabbit anti-rat HRP- or goat anti-rabbit HRP-conjugated secondary antibody, respectively (Bio-rad Laboratories, Hercules, CA) and the DAB peroxidase substrate kit (Vector Laboratories, Inc. Burlingame, CA). Sections were then counterstained with hematoxylin. Tissue sections were blindly quantified by manual

counting. Representative areas^{2,3} from each CD31 stained section ($n = 12$ in total) with most intensive microvessel density was captured under the light microscope at 200x (Leica). MVD per tumor section was calculated from the average count of CD31⁺ vessels per representative area, averaging total number from $n = 3$ tumors per treatment group. Total image length is 384 μm . Immunofluorescence was performed using rat mAb CD4 (GK1.5, Abcam, Cambridge, MA) and rabbit pAb CD8 antibodies (ab4055, Abcam). Sections were examined with a Nikon microscope and camera and processed in ImageJ.

Flow cytometry

Tumor-infiltrating immune cells were isolated and stained with fluorochrome-conjugated mAbs specific for mouse surface markers CD45, CD44, CD8, CD4, Nk1.1, CD11b, CD11c, Ly6C, Ly6G, CD19, TCR β , F4/80 (BD Biosciences, Ebioscience/Thermo Fisher Scientific) according to standard procedures. Intracellular staining (*T cell Stimulation*) for IFN γ , and Ki-67 and granzyme-B was performed after permeabilization of cell membranes using the Transcription Factor Staining Buffer Set from ebioscience (ThermoFisher). All samples were run on a BD LSRFortessa unit and analyzed by FlowJoX software (Flowjo LLC, Ashland, OR).

Reverse transcriptase PCR

Tumor samples were harvested and immediately snap-frozen in liquid nitrogen. Total RNA was isolated using the mirVana miRNA isolation kit with phenol (Ambion [Thermo Fisher Scientific], Carlsbad, CA) with concentration measured on the NanoDrop ND-1000 Spectrophotometer. One-step quantitative reverse transcriptase PCR was performed with diluted RNA, AgPath-ID One-step reverse transcriptase PCR reagents, and Taqman gene expression assay primers (Thermo Fisher Scientific) for the genes indicated, using relative expression of GAPDH as a reference gene. Samples were analyzed on the StepOnePlus Real-Time PCR System with StepOne Software v2.3 (Applied Biosystems [Thermo Fisher Scientific]).

RNA-seq of murine tumors

Stranded Total RNA sequencing was performed by the MD Anderson Sequencing and Microarray Facility (SMF) on the Illumina Hi-Seq 4000 platform. RNA samples were isolated from MB49 tumors using the mirVana miRNA isolation kit with phenol (Ambion [Thermo Fisher Scientific]), confirmed purity and concentration by the Agilent 2100 Bioanalyzer (Agilent Technologies [Thermo Fisher Scientific]) and Nanodrop ND-1000 Spectrophotometer, and sent to SMF. Raw reads in FASTQ format were aligned to the mouse reference genome, GRCm38/mm10, using MOSAIK²⁵ alignment software. Mapped reads were used to generate raw counts for each gene using HTSeq. Counts data were normalized across samples with DESeq⁵⁰ and normalized expression values were analyzed by Morpheus matrix visualization and analysis software (Broad Institute) and Gene Set Enrichment Analysis (GSEA) software (Broad Institute). The up-regulated

pathways in GSEA were defined by a normalized enrichment score (NES) >0 . Only the top 20 pathways more enriched in each treatment group were listed.

Urinary cytokine analysis

Frozen patient urines collected from baseline Day 1 (D1) pre-treatment, and Day 4 and Day 12 (D4, D12) post-treatment of Phase I and II clinical trials with Instiladrin (Ad-IFN α /Syn3) by the SUOCTC working group were thawed and diluted before analysis with the Bio-Plex ProTM Cytokine, Chemokine, and Growth Factor Assay Kit (Bio-Rad Laboratories, Inc., Hercules, CA). We utilized antibody targets from the Human Cytokine Standard Groups I and II. Samples were run in duplicate, and the plate was read with Bio-Plex ManagerTM software (Bio-Rad Laboratories, Inc) in the MD Anderson Department of Surgery. Observed concentration was log₂ transformed, and graphed with baseline corrected to Day 1 levels of each cytokine. Patients with undetectable levels of cytokines were left out of analyses. *Assessment:* of the 39 total patients, 13 were deemed as “responders” (CR) as defined by no evidence of recurrence of a high-grade tumor by cystoscopy, cytology, or if clinically indicated, biopsy at 12 months. The other 26 patients were deemed “non-responders” (NR). Correlation between IFN α 2 levels and other cytokines were deemed as moderately positive if $r > 0.5$ and strongly positive if $r > 0.7$. Positive correlation was considered statistically significant if p -value <0.05 .

Analyses of gene expression for patients treated with Ad-IFN α

RNA isolation

The tumor areas in formalin fixed, paraffin-embedded (FFPE) human specimens from the Phase I, Ib, and II trials with Instiladrin (Ad-IFN α /Syn3) were reviewed by a genitourinary pathologist. Total RNA from 8 matched (16 total) FFPE tumors was isolated using the High Pure miRNA isolation kit (Roche, Indianapolis, IN) according to the manufacturer's instructions. Briefly, for the deparaffinization, five to ten (depending on the tumor area) 10 μm sections were incubated with xylene for 5 min, followed by two ethanol washes and dried for 10 min at 55° C. The dried tissues were incubated with proteinase K for 3 h at 55°C degree, followed by two washes according to the instructions of the manufacturer. RNA was eluted with water and treated with DNase for 30 min at 37°C. DNase treated RNA was washed twice according to the manufacturer's instructions and eluted with water. RNA purity and integrity was measured by NanoDrop ND-1000 and Agilent 2100 Bioanalyzer and only high-quality RNA was used for library preparation.

Library preparation and sequencing

Whole transcriptome RNA sequencing was performed using Ion Torrent's AmpliseqRNA platform (Thermo Fisher Scientific) and an Ion Proton sequencer (Thermo Fisher Scientific). Twenty nanograms of purified RNA was transcribed into cDNA using the SuperScript[®] VILO[™] kit. Then cDNA was amplified using the Ion Ampliseq Transcriptome Human Gene Expression Core panel, followed by ligation of

adapters and barcodes to amplicons and purification. Purified libraries were quantified using the Ion Library Quantification kit (Thermo Fisher Scientific) according to the manufacturer's instructions. Libraries were diluted to 100 pM and pooled in sets of eight. Pooled libraries were amplified on Ion SphereTM particles (ISP) using emulsion PCR and enriched on the IonChef (Thermo Fisher Scientific). Template positive ISPs were loaded into Ion PI chips and run on the Proton instrument in the Genomics Core in the Department of Urology at The University of Texas MD Anderson Cancer Center.

Bioinformatics Analysis

RNA-Seq gene expression analysis: Primary analysis of RNA sequencing data was performed using AmpliSeqRNA analysis plugin in the Torrent Suite Software. This plugin aligned the raw sequence reads to a human reference genome that contains 20,802 RefSeq transcripts (hg19 Ampliseq Transcriptome_ERCC_V1.fasta) using the Torrent Mapping Alignment Program (TMAP). Then, the number of reads mapped per gene will be counted to generate raw counts files and normalized reads per gene per million mapped reads (RPM) files. To visualize expression patterns, log ratios of POST/PRE gene expression of matched tumors were used for hierarchical clustering with Cluster and TreeView,⁵¹ or log₂ normalized expression values were analyzed by Morpheus matrix visualization and analysis software (Broad Institute). *Assessment:* of the eight total patients analyzed, none were classified as "responders" (CR) as defined by no evidence of recurrence of a high-grade tumor by cystoscopy, cytology, or if clinically indicated, biopsy at 12 months.

Statistical analyses

Statistical analyses of experimental results were evaluated with the GraphPad Prism 7 software. Two-tailed Student *t* tests, log-rank analyses, or multiple unpaired *t* tests were performed using averaged treatment group measurements at any one time point, as indicated. One way ANOVA with multiple comparisons was used for patient urine samples for each cytokine. Results were considered statistically significant when *, *P* < 0.05; **, *P* < 0.01; ***, *P* < 0.001.

Acknowledgments

We are grateful to Dr. Xiaoping Su and MD Anderson SMF Core Laboratory for their work in sequencing, aligning, and normalizing the RNA data; Dr. William Kim and his lab at University of North Carolina Chappell Hill for their donation of BBN and UPPL-mouse-derived murine bladder cancer cell lines and discussion for experimental aid; Shelley Herbrich for help with GSEA and statistical analysis; Rosa Santana, Sarai Rivas, Shweta Hedge for invaluable discussions and experimental aid; and MD Anderson Department of Scientific Publications, specifically Erica Goodoff for preliminary editing of this manuscript.

Special thanks to the Clinical Investigators associated with the Society of Urologic Oncology Clinical Trials Consortium and who participated in the Phase 2 study, including: Dr. Trinity Bivalacqua of Johns Hopkins Medical Center, Dr. Stephen Boorjian of the Mayo Clinic, Dr. Daniel Canter of the Oschner Clinic, Dr. Tracey Downs of the University of Wisconsin Medical Center, Dr. Leonard Gomella of Thomas Jefferson

University, Dr. Robert Grubb III of the Medical University of South Carolina, Dr. Brant Inman of Duke University Medical Center, Dr. Ashish Kamat of MD Anderson Cancer Center, Dr. Larry Karsh of the Urology Center of Colorado, Dr. Tracey Krupski of the University of Virginia, Dr. Seth Lerner of Baylor College of Medicine, Dr. Yair Lotan of the University of Texas Southwestern Medical Center, Dr. Matthew Milowsky of the University of North Carolina Medical Center, Dr. Kenneth Ogan of Emory Clinic, Dr. Neal Shore of the Carolina Urologic Research Center, Dr. Robert Svatek of the University of Texas Health Science Center San Antonio, and Dr. Michael Woods of Loyola University Medical Center.

Disclosure of Potential Conflicts of Interests

Colin P. Dinney is the Independent Chairman of the Steering Committee for FKD Therapies Oy for the Phase III Instiladrin trial.

Funding

This research was supported in part by FKD Therapies Oy (Kuopio, Finland), A.I. Virtanen Institute for Molecular Sciences (Kuopio, Finland), and grants from National Institutes of Health/National Cancer Institute (P50 CA091846), MD Anderson CCSG program (P30 016672), and the Cancer Prevention Research Institute of Texas (RP160188 to K.S.S)

Authors Contributions

Study concept and design: C. Dinney

Acquisition of data: D. Plote, S. Mokkalapati, W. Choi, J. Ferguson, D. Sundi, N. Parker, S. Yla-Herttuala, SUOCTC Research Group

Analysis and interpretation of data: D. Plote, S. Mokkalapati, W. Choi, K. Schluns

Writing manuscript: D. Plote, S. Mokkalapati, J. Duplisea, W. Choi, K. Schluns, C. Dinney

Statistical analysis: D. Plote

Administrative, technical or material support: SUOCTC Research Group

ORCID

Devin Plote  <http://orcid.org/0000-0002-7715-4142>

Sharada Mokkalapati  <http://orcid.org/0000-0001-5325-5574>

Debasish Sundi  <http://orcid.org/0000-0001-6980-4777>

James E Ferguson  <http://orcid.org/0000-0001-9073-9615>

SUO CTC Bladder Committee  <http://orcid.org/0000-0001-7593-2708>

Kimberly S. Schluns  <http://orcid.org/0000-0002-3738-2853>

Colin P. Dinney  <http://orcid.org/0000-0002-8969-711X>

References

1. Knowles MA, Hurst CD. Molecular biology of bladder cancer: new insights into pathogenesis and clinical diversity. *Nat Rev Cancer*. 2015;15(1):25–41. doi:10.1038/nrc3817. PubMed PMID: 25533674.
2. Singh P, Black P. Emerging role of checkpoint inhibition in localized bladder cancer. *Urol Oncol*. 2016;34(12):548–555. doi:10.1016/j.urolonc.2016.09.004. PubMed PMID: 27776977.
3. Lamm DL, Blumenstein BA, Crissman JD, Montie JE, Gottesman JE, Lowe BA, Sarosdy MF, Bohl RD, Grossman HB, Beck TM, et al. Maintenance bacillus calmette-guerin immunotherapy for recurrent ta, t1 and carcinoma in situ transitional cell carcinoma of the bladder: a randomized southwest oncology group study. *J Urol*. 2000;163(4):1124–1129. PubMed PMID: 10737480.
4. Dalbagni G, Russo P, Sheinfeld J, Mazumdar M, Tong W, Rabbani F, Donat MS, Herr HW, Sogani P, dePalma D, et al.

- Phase I trial of intravesical gemcitabine in bacillus calmette-guerin-refractory transitional-cell carcinoma of the bladder. *J Clin Oncol.* 2002;20(15):3193–3198. doi:10.1200/JCO.2002.02.066. PubMed PMID: 12149290.
5. von Rundstedt FC, Lerner SP. Bacille-calmette-guerin non-responders: how to manage. *Transl Androl Urol.* 2015;4(3):244–253. doi:10.3978/j.issn.2223-4683.2015.05.03. PubMed PMID: 26816828; PubMed Central PMCID: PMC4708234.
 6. Zlotta AR, Fleshner NE, Jewett MA. The management of bcg failure in non-muscle-invasive bladder cancer: an update. *Can Urol Assoc J.* 2009;3(6 Suppl 4):S199–205. PubMed PMID: 20019985; PubMed Central PMCID: PMC2792453.
 7. Lamm D, Brausi M, Ma O, Witjes JA. Interferon alfa in the treatment paradigm for non-muscle-invasive bladder cancer. *Urol Oncol.* 2014;32(1):35 e21–30. doi:10.1016/j.urolonc.2013.02.010. PubMed PMID: 23628309.
 8. Dinney CP, Fisher MB, Navai N, Ma O, Cutler D, Abraham A, Young S, Hutchins B, Caceres M, Kishnani N, et al. Phase I trial of intravesical recombinant adenovirus mediated interferon-alpha2b formulated in syn3 for bacillus calmette-guerin failures in non-muscle invasive bladder cancer. *J Urol.* 2013;190(3):850–856. doi:10.1016/j.juro.2013.03.030. PubMed PMID: 23507396; PubMed Central PMCID: PMC3951790.
 9. Shore ND, Boorjian SA, Canter DJ, Ogan K, Li K, Downs TM, Gomella LG, Kamat AM, Lotan Y, Svatek RS, et al. Intravesical rad-ifnalpha/syn3 for patients with high-grade, bacillus calmette-guerin-refractory or relapsed non-muscle-invasive bladder cancer: a phase II randomized study. *J Clin Oncol.* 2017;35(30):3410–3416. doi:10.1200/JCO.2017.72.3064. PubMed PMID: 28834453; PubMed Central PMCID: PMC5648171.
 10. Navai N, Benedict WF, Zhang G, Abraham A, Ainslie N, Shah JB, Hb G, Am K, Cp D. Phase Ib trial to evaluate tissue response to a second dose of intravesical recombinant adenoviral interferon alpha2b formulated in syn3 for failures of bacillus calmette-guerin (bcg) therapy in nonmuscle invasive bladder cancer. *Ann Surg Oncol.* 2016;23(12):4110–4114. doi:10.1245/s10434-016-5300-6. PubMed PMID: 27387678; PubMed Central PMCID: PMC5459317.
 11. Papageorgiou A, Dinney CP, McConkey DJ. Interferon-alpha induces trail expression and cell death via an irf-1-dependent mechanism in human bladder cancer cells. *Cancer Biol Ther.* 2007;6(6):872–879. PubMed PMID: 17617740.
 12. Ji I, Sweeney P, Perrotte P, Kedar D, Dong Z, Jw S, Karashima T, Inoue K, Wf B, Cp D. Inhibition of tumorigenicity and metastasis of human bladder cancer growing in athymic mice by interferon-beta gene therapy results partially from various antiangiogenic effects including endothelial cell apoptosis. *Clin Cancer Res.* 2002;8(4):1258–1270. PubMed PMID: 11948141.
 13. von Marschall Z, Scholz A, Cramer T, Schafer G, Schirner M, Oberg K, Wiedenmann B, Hocker M, Rosewicz S. Effects of interferon alpha on vascular endothelial growth factor gene transcription and tumor angiogenesis. *J Natl Cancer Inst.* 2003;95(6):437–448. PubMed PMID: 12644537.
 14. Dinney CP, Bielenberg DR, Perrotte P, Reich R, Eve BY, Bucana CD, Fidler IJ. Inhibition of basic fibroblast growth factor expression, angiogenesis, and growth of human bladder carcinoma in mice by systemic interferon-alpha administration. *Cancer Res.* 1998;58(4):808–814. PubMed PMID: 9485039.
 15. Benedict WF, Tao Z, Kim CS, Zhang X, Jh Z, Adam L, Dj M, Papageorgiou A, Munsell M, Philopena J, et al. Intravesical ad-ifnalpha causes marked regression of human bladder cancer growing orthotopically in nude mice and overcomes resistance to ifn-alpha protein. *Mol Ther.* 2004;10(3):525–532. doi:10.1016/j.ymthe.2004.05.027. PubMed PMID: 15336652.
 16. Parkin J, Cohen B. An overview of the immune system. *Lancet.* 2001;357(9270):1777–1789. doi:10.1016/S0140-6736(00)04904-7. PubMed PMID: 11403834.
 17. Hervas-Stubbs S, Ji P-G, Rouzaut A, Mf S, Le BA, Melero I. Direct effects of type I interferons on cells of the immune system. *Clin Cancer Res.* 2011;17(9):2619–2627. doi:10.1158/1078-0432.CCR-10-1114. PubMed PMID: 21372217.
 18. Bald T, Landsberg J, Lopez-Ramos D, Renn M, Glodde N, Jansen P, Gaffal E, Steitz J, Tolba R, Kalinke U, et al. Immune cell-poor melanomas benefit from pd-1 blockade after targeted type I ifn activation. *Cancer Discov.* 2014;4(6):674–687. doi:10.1158/2159-8290.CD-13-0458. PubMed PMID: 24589924.
 19. Terawaki S, Chikuma S, Shibayama S, Hayashi T, Yoshida T, Okazaki T, Honjo T. Ifn-alpha directly promotes programmed cell death-1 transcription and limits the duration of t cell-mediated immunity. *J Immunol.* 2011;186(5):2772–2779. doi:10.4049/jimmunol.1003208. PubMed PMID: 21263073.
 20. Garcia-Diaz A, Shin DS, Moreno BH, Saco J, Escuin-Ordinas H, Rodriguez GA, Zaretsky JM, Sun L, Hugo W, Wang X, et al. Interferon receptor signaling pathways regulating pd-1 and pd-l2 expression. *Cell Rep.* 2017;19(6):1189–1201. doi:10.1016/j.celrep.2017.04.031. PubMed PMID: 28494868.
 21. Ribas A. Adaptive immune resistance: how cancer protects from immune attack. *Cancer Discov.* 2015;5(9):915–919. doi:10.1158/2159-8290.CD-15-0563. PubMed PMID: 26272491; PubMed Central PMCID: PMC4560619.
 22. Pardoll DM. The blockade of immune checkpoints in cancer immunotherapy. *Nat Rev Cancer.* 2012;12(4):252–264. doi:10.1038/nrc3239. PubMed PMID: 22437870; PubMed Central PMCID: PMC4856023.
 23. Zaretsky JM, Garcia-Diaz A, Shin DS, Escuin-Ordinas H, Hugo W, Hu-Lieskovan S, Torrejon DY, Abril-Rodriguez G, Sandoval S, Barthly L, et al. Mutations associated with acquired resistance to pd-1 blockade in melanoma. *N Engl J Med.* 2016;375(9):819–829. doi:10.1056/NEJMoa1604958. PubMed PMID: 27433843; PubMed Central PMCID: PMC5007206.
 24. Gao J, Shi LZ, Zhao H, Chen J, Xiong L, He Q, Chen T, Roszik J, Bernatchez C, Se W, et al. Loss of ifn-gamma pathway genes in tumor cells as a mechanism of resistance to anti-ctla-4 therapy. *Cell.* 2016;167(2):397–404 e9. doi:10.1016/j.cell.2016.08.069. PubMed PMID: 27667683; PubMed Central PMCID: PMC5088716.
 25. Multhoff G, Molls M, Radons J. Chronic inflammation in cancer development. *Front Immunol.* 2011;2:98. doi:10.3389/fimmu.2011.00098. PubMed PMID: 22566887; PubMed Central PMCID: PMC3342348.
 26. Vandever AJ, Fallon JK, Tighe R, Sabzevari H, Schlom J, Greiner JW. Systemic immunotherapy of non-muscle invasive mouse bladder cancer with avelumab, an anti-pd-1 immune checkpoint inhibitor. *Cancer Immunol Res.* 2016;4(5):452–462. doi:10.1158/2326-6066.CIR-15-0176. PubMed PMID: 26921031; PubMed Central PMCID: PMC4881865.
 27. Saito R, Smith CC, Utsumi T, Bixby LM, Kardos J, Wobker SE, Stewart KG, Chai S, Manocha U, Byrd KM, et al. Molecular subtype-specific immunocompetent models of high-grade urothelial carcinoma reveal differential neoantigen expression and response to immunotherapy. *Cancer Res.* 2018;78(14):3954–3968. doi:10.1158/0008-5472.CAN-18-0173. PubMed PMID: 29784854; PubMed Central PMCID: PMC6157276.
 28. Guo Y, Luan L, Rabacal W, Bohannon JK, Fensterheim BA, Hernandez A, Sherwood ER. Il-15 superagonist-mediated immunotoxicity: role of nk cells and ifn-gamma. *J Immunol.* 2015;195(5):2353–2364. doi:10.4049/jimmunol.1500300. PubMed PMID: 26216888; PubMed Central PMCID: PMC4543906.
 29. Shime H, Matsumoto M, Seya T. Double-stranded rna promotes ctl-independent tumor cytotoxicity mediated by cd11b(+)ly6g(+) intratumor myeloid cells through the ticam-1 signaling pathway. *Cell Death Differ.* 2017;24(3):385–396. doi:10.1038/cdd.2016.131. PubMed PMID: 27834952; PubMed Central PMCID: PMC5344202.
 30. Trinchieri G. Interleukin-12 and the regulation of innate resistance and adaptive immunity. *Nat Rev Immunol.* 2003;3(2):133–146. doi:10.1038/nri1001. PubMed PMID: 12563297.
 31. Heufler C, Koch F, Stanzl U, Topar G, Wysocka M, Trinchieri G, Enk A, Rm S, Romani N, Schuler G. Interleukin-12 is produced by

- dendritic cells and mediates t helper 1 development as well as interferon-gamma production by t helper 1 cells. *Eur J Immunol.* **1996**;26(3):659–668. doi:10.1002/eji.1830260323. PubMed PMID: 8605935.
32. van Hooren L, Sandin LC, Moskalev I, Ellmark P, Dimberg A, Black P, Totterman TH, Mangsbo SM. Local checkpoint inhibition of ctla-4 as a monotherapy or in combination with anti-pd1 prevents the growth of murine bladder cancer. *Eur J Immunol.* **2017**;47(2):385–393. doi:10.1002/eji.201646583. PubMed PMID: 27873300.
 33. Muthuswamy R, Wang L, Pitteroff J, Gingrich JR, Kalinski P. Combination of ifnalpha and poly-i: creprograms bladder cancer microenvironment for enhanced ctl attraction. *J Immunother Cancer.* **2015**;3:6. doi:10.1186/s40425-015-0050-8. PubMed PMID: 25806105; PubMed Central PMCID: PMC4371844.
 34. Rincon M. Interleukin-6: from an inflammatory marker to a target for inflammatory diseases. *Trends Immunol.* **2012**;33(11):571–577. doi:10.1016/j.it.2012.07.003. PubMed PMID: 22883707.
 35. Allen E, Jabouille A, Rivera LB, Lodewijckx I, Missiaen R, Steri V, Feyen K, Tawney J, Hanahan D, Michael IP, et al. Combined antiangiogenic and anti-pd-1 therapy stimulates tumor immunity through hev formation. *Sci Transl Med.* **2017**;9(385). doi:10.1126/scitranslmed.aak9679. PubMed PMID: 28404866; PubMed Central PMCID: PMC5554432.
 36. Rv D, Harrison K, Oyston PC, Lukaszewski RA, Clark GC. Targeting the “cytokine storm” for therapeutic benefit. *Clin Vaccine Immunol.* **2013**;20(3):319–327. doi:10.1128/COI.00636-12. PubMed PMID: 23283640; PubMed Central PMCID: PMC3592351.
 37. Tisoncik JR, Korth MJ, Simmons CP, Farrar J, Martin TR, Katze MG. Into the eye of the cytokine storm. *Microbiol Mol Biol Rev.* **2012**;76(1):16–32. doi:10.1128/MMBR.05015-11. PubMed PMID: 22390970; PubMed Central PMCID: PMC3294426.
 38. Kim KD, Zhao J, Auh S, Yang X, Du P, Tang H, Fu YX. Adaptive immune cells temper initial innate responses. *Nat Med.* **2007**;13(10):1248–1252. doi:10.1038/nm1633. PubMed PMID: 17891146; PubMed Central PMCID: PMC2435248.
 39. Lu Z, Xu S. Erk1/2 map kinases in cell survival and apoptosis. *IUBMB Life.* **2006**;58(11):621–631. doi:10.1080/15216540600957438. PubMed PMID: 17085381.
 40. Patsoukis N, Bardhan K, Chatterjee P, Sari D, Liu B, Ln B, Ed K, Gj F, Petkova V, Seth P, et al. Pd-1 alters t-cell metabolic reprogramming by inhibiting glycolysis and promoting lipolysis and fatty acid oxidation. *Nat Commun.* **2015**;6:6692. doi:10.1038/ncomms7692. PubMed PMID: 25809635; PubMed Central PMCID: PMC4389235.
 41. Chang CH, Qiu J, O’Sullivan D, Buck MD, Noguchi T, Curtis JD, Chen Q, Gindin M, Gubin MM, van der Windt GJ, et al. Metabolic competition in the tumor microenvironment is a driver of cancer progression. *Cell.* **2015**;162(6):1229–1241. doi:10.1016/j.cell.2015.08.016. PubMed PMID: 26321679; PubMed Central PMCID: PMC4864363.
 42. O’Sullivan D, van der Windt GJ, Huang SC, Curtis JD, Chang CH, Buck MD, Qiu J, Smith AM, Lam WY, DiPlato LM, et al. Memory cd8(+) t cells use cell-intrinsic lipolysis to support the metabolic programming necessary for development. *Immunity.* **2014**;41(1):75–88. doi:10.1016/j.immuni.2014.06.005. PubMed PMID: 25001241; PubMed Central PMCID: PMC4120664.
 43. Pearce EL, Walsh MC, Cejas PJ, Harms GM, Shen H, Wang LS, Jones RG, Choi Y. Enhancing cd8 t-cell memory by modulating fatty acid metabolism. *Nature.* **2009**;460(7251):103–107. doi:10.1038/nature08097. PubMed PMID: 19494812; PubMed Central PMCID: PMC2803086.
 44. LA O, Kishton RJ, Rathmell J. A guide to immunometabolism for immunologists. *Nat Rev Immunol.* **2016**;16(9):553–565. doi:10.1038/nri.2016.70. PubMed PMID: 27396447; PubMed Central PMCID: PMC5001910.
 45. Hugo W, Zaretsky JM, Sun L, Song C, Moreno BH, Huelieskovan S, Berent-Maoz B, Pang J, Chmielowski B, Cherry G, et al. Genomic and transcriptomic features of response to anti-pd-1 therapy in metastatic melanoma. *Cell.* **2016**;165(1):35–44. doi:10.1016/j.cell.2016.02.065. PubMed PMID: 26997480; PubMed Central PMCID: PMC4808437.
 46. Davarpanah NN, Yuno A, Trepel JB, Ab A. Immunotherapy: A new treatment paradigm in bladder cancer. *Curr Opin Oncol.* **2017**. doi:10.1097/CCO.0000000000000366. PubMed PMID: 28306559; PubMed Central PMCID: PMC5526432.
 47. Zhang ZT, Pak J, Huang HY, Shapiro E, Sun TT, Pellicer A, Wu XR. Role of ha-ras activation in superficial papillary pathway of urothelial tumor formation. *Oncogene.* **2001**;20(16):1973–1980. doi:10.1038/sj.onc.1204315. PubMed PMID: 11360181.
 48. Weskamp G, Mendelson K, Swendeman S, Le GS, Ma Y, Lyman S, Hinoki A, Eguchi S, Guaiquil V, Horiuchi K, et al. Pathological neovascularization is reduced by inactivation of adam17 in endothelial cells but not in pericytes. *Circ Res.* **2010**;106(5):932–940. doi:10.1161/CIRCRESAHA.109.207415. PubMed PMID: 20110534; PubMed Central PMCID: PMC2842448.
 49. Lodolce JP, Boone DL, Chai S, Re S, Dassopoulos T, Trettin S, Ma A. Il-15 receptor maintains lymphoid homeostasis by supporting lymphocyte homing and proliferation. *Immunity.* **1998**;9(5):669–676. PubMed PMID: 9846488.
 50. Lee WP, Stromberg MP, Ward A, Stewart C, Garrison EP, Marth GT. Mosaik: a hash-based algorithm for accurate next-generation sequencing short-read mapping. *PLoS One.* **2014**;9(3):e90581. doi:10.1371/journal.pone.0090581. PubMed PMID: 24599324; PubMed Central PMCID: PMC3944147.
 51. Eisen MB, Spellman PT, Brown PO, Botstein D. Cluster analysis and display of genome-wide expression patterns. *Proc Natl Acad Sci U S A.* **1998**;95(25):14863–14868. PubMed PMID: 9843981; PubMed Central PMCID: PMC24541.